Precambrian Research 393 (2023) 107077

Contents lists available at ScienceDirect

Precambrian Research

journal homepage: www.elsevier.com/locate/precamres

One billion years of tectonism at the Paleoproterozoic interface of North and South Australia

Laura J. Morrissey [a,b,*], Justin L. Payne [c,b], Martin Hand [d,b], Chris Clark [e,b], Matthew Janicki [c]

[a] Future Industries Institute, University of South Australia, Mawson Lakes, SA 5095, Australia
[b] Mineral Exploration Cooperative Research Centre, Kensington, WA 6151, Australia
[c] UniSA STEM, University of South Australia, Mawson Lakes, SA 5095, Australia
[d] Department of Earth Sciences, University of Adelaide, Adelaide, SA 5005, Australia
[e] School of Earth and Planetary Sciences, Curtin University, Perth, WA 6845, Australia

A B S T R A C T

The Mount Woods Domain, in the northeastern Gawler Craton, occupies a tectonically important location in Proterozoic Australia, yet there is very little published U–Pb geochronology data from this region to underpin tectonic models. New LA-ICP-MS U–Pb monazite and detrital zircon geochronology reveal Archean to Paleoproterozoic basement in the central Mount Woods Domain, comprising metasedimentary rocks and garnet-bearing granite with protolith ages of c. 2550–2400 Ma and metasedimentary rocks deposited after c. 1855 Ma. The southern Mount Woods Domain contains younger metasedimentary sequences deposited after 1750 Ma. Metamorphic monazite and zircon geochronology combined with phase equilibria modelling show the rocks of the central Mount Woods Domain were metamorphosed to granulite facies between 1700 and 1670 Ma, reaching pressure and temperature conditions of 4.8–5.3 kbar and 800–840 °C. Monazite geochronology from samples located along major shear zones and in the westernmost Mount Woods Domain record amphibolite facies metamorphism and reworking at 1570–1550 Ma, with a further phase of shear zone activity along the northern margin of the Mount Woods Domain at c. 1480 Ma. Laser ablation inductively coupled plasma triple quadrupole mass spectrometry (LA-ICP-QQQ-MS) Rb–Sr biotite ages from across the Mount Woods Domain range between 1480 and 1390 Ma. The protracted geological history in the Mount Woods Domain from c. 2500–1400 Ma provides a piercing point linking different regions of Proterozoic Australia and western Laurentia during the tenure of the Nuna supercontinent.

1. Introduction

Archean–Proterozoic Australia and East Antarctica are important components of the Nuna and Rodinia supercontinents in the Paleo to Mesoproterozoic (Fig. 1a). A connection between Australia, Laurentia and Antarctica in the Mesoproterozoic has long been proposed based on provenance studies in Laurentian sedimentary rocks deposited after c. 1500 Ma (e.g. Daniel et al., 2013; Medig et al., 2014; Ross and Villeneuve, 2003), with recent studies from north-eastern Australia proposing that eastern Australia and Laurentia amalgamated around c. 1600 Ma (e.g. Pourteau et al., 2018; Volante et al., 2020). Paleomagnetic data have been used to provide a variety of "best-fit" models for these timelines (e.g. Kirscher et al., 2020; Pehrsson et al., 2015; Pisarevsky et al., 2014). However, a number of reconstruction models also suggest links between Australia and Laurentia in the late Paleoproterozoic (c. 1800–1700 Ma) based on detrital zircon provenance and temporal correlations between phases of sedimentation and major tectonic events (e.g. Betts et al., 2008; Holland et al., 2018; Payne et al., 2009). Assessing the validity of these correlations and testing models for the amalgamation of Australia and Laurentia within the Nuna supercontinent requires a clear understanding of the timing and character of tectonic events at a craton-scale within Australia. This is currently hindered by a lack of understanding of the geological history of poorly exposed parts of Australia. This poor understanding has also led to contrasting views as to the importance of reworking of coherent continental crust (e.g. Cawood and Korsch, 2008; Payne et al., 2009) versus accretion of multiple continental ribbons (e.g. Betts et al., 2016) in the evolution of the Australian continent.

The poorly exposed Mount Woods Domain, in the northeastern Gawler Craton, sits inboard from the inferred Proterozoic eastern margin of Australia (Fig. 1c) and is a key region for understanding the ancient connections between the modern-day North and South Australian Cratons (NAC and SAC). Importantly it sits at the interface between the so-called "Archean nucleus" of the Gawler Craton and regions to the north that are often considered equivalent to or connected to the Aileron Province in the NAC (Armit et al., 2017; Payne et al., 2008). The different regions of the northern Gawler Craton appear to record different metamorphic histories. The Nawa Domain dominantly records

* Corresponding author.
E-mail address: laura.morrissey@unisa.edu.au (L.J. Morrissey).

https://doi.org/10.1016/j.precamres.2023.107077
Received 30 September 2022; Received in revised form 8 March 2023; Accepted 4 May 2023
Available online 22 May 2023

metamorphism at c. 1700 Ma (Payne et al., 2008), with spatially localised events at c. 1520 Ma and c. 1450 Ma (Morrissey et al., 2019; Reid et al., 2014a), whereas the Coober Pedy and Mabel Creek Ridge regions dominantly record metamorphism at 1600–1550 Ma (Cutts et al., 2011; Payne et al., 2008). Although there is very little published geochronology from the Mount Woods Domain, previous studies have hinted that the region has the potential to record both Paleoproterozoic and early Mesoproterozoic events (e.g. Betts et al., 2003; Forbes et al., 2011; Tiddy et al., 2020) and can therefore act as tie points between potentially disparate crustal blocks.

To explore the metamorphic architecture of the Mount Woods Domain, and its affinities with the wider Australian and Laurentian crust, we combine LA-ICP-MS U–Pb detrital zircon geochronology, metamorphic monazite and zircon geochronology, Rb-Sr geochronology, petrology and phase equilibria modelling. This is done to determine the protolith ages and metamorphic history from across the buried extent of the Mount Woods Domain. This approach identifies a late Archean to earliest Paleoproterozoic basement that has experienced multiple cycles of sedimentation and metamorphism extending from the amalgamation to the onset of breakup of the Nuna supercontinent.

2. Geological setting

Proterozoic Australia has been divided into three cratonic elements based on present-day geography: the North, South and West Australian Cratons (NAC, SAC and WAC; Fig. 1b). Recent work has shown the WAC only amalgamated with the NAC and SAC after c. 1370 Ma (Payne et al., 2021), so is not considered further in this study. The NAC and SAC share a Paleoproterozoic history and are thought to have rotated into their current, separate positions after c. 1450 Ma (Cawood and Korsch, 2008;

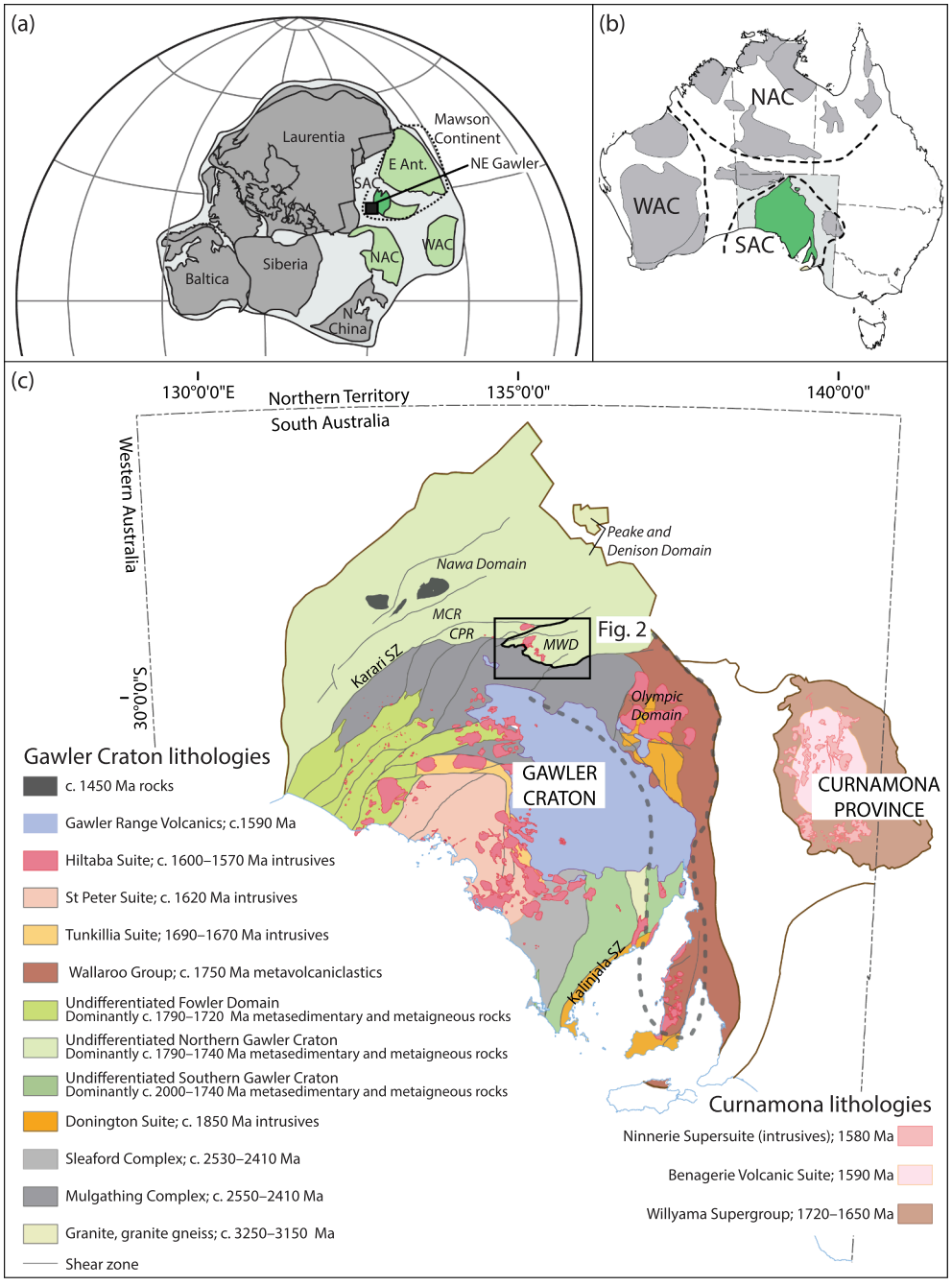

Fig. 1. (a) Reconstruction of the Nuna supercontinent at c. 1650 Ma, after Kirscher et al., (2020). The three Australian cratons (north, west and south; NAC, WAC and SAC) are shown in shades of green with the Gawler Craton shown as dark green. The position of the northeastern Gawler Craton is shown as a black square. The South Australian Craton (SAC) and East Antarctica (E. Ant) together comprise the Mawson Continent (dashed line), after Payne et al., 2009. (b) The Gawler Craton (green) shown in context with Precambrian basement terranes (grey) within Australia. (c) Simplified interpreted solid geology map of the Gawler Craton, after Reid et al. (2014a). The Mount Woods Domain (MWD) is shown by a bold outline. Other shear-bound domains in the northern Gawler Craton are also shown; Coober Pedy Ridge (CPR), Mabel Creek Ridge (MCR) and Nawa Domain. (For interpretation of the references to colour in this figure legend, the reader is referred to the web version of this article.)

Payne et al., 2009). The SAC comprises the Gawler Craton and Curnamona Province, and correlates with Terre Adelie Land in East Antarctica (Fig. 1).

The basement of the Gawler Craton consists of c. 3250–3150 Ma granitic gneiss, and metasedimentary and metaigneous rocks of the Sleaford and Mulgathing Complexes, which have protolith ages of 2555–2440 Ma (Fig. 1c; Fraser et al., 2010; Reid et al., 2014b; Swain et al., 2005). The Sleaford and Mulgathing Complexes are interpreted to represent parts of a contiguous late Archean belt. The basement rocks were deformed and metamorphosed during the 2465–2415 Ma Sleafordian Orogeny (Daly et al., 1998; Dutch et al., 2010; Halpin and Reid, 2016; McFarlane, 2006; Reid et al., 2014b). Between 2000 and 1730 Ma the tectonic setting of the Gawler Craton was dominantly extensional, resulting in the deposition of a number of volcanoclastic sedimentary sequences (Fig. 1; Fanning et al., 2007; Hand et al., 2007; Howard et al., 2011a; Lane et al., 2015; Payne et al., 2006; Reid and Hand, 2012; Szpunar et al., 2011). Widespread basin development and sedimentation was succeeded by the Kimban Orogeny at c. 1730–1690 Ma, which involved the development of crustal-scale shear zones, granitic magmatism and widespread metamorphism (e.g. Dutch et al., 2008; Dutch et al., 2010; Fanning et al., 2007; Hand et al., 2007; Howard et al., 2011b; Morrissey et al., 2016b; Payne et al., 2008; Vassallo and Wilson, 2002). The Kimban Orogeny was followed by extensive magmatic activity across the Gawler Craton, with the formation of the c. 1690–1670 Ma Tunkillia Suite (Hand et al., 2007; Payne et al., 2010), the c. 1620 Ma St Peter Suite (Reid et al., 2020; Swain et al., 2008) and development of a felsic large igneous province that includes the 1600–1570 Ma Hiltaba Suite granites, voluminous c. 1592 Ma Gawler Range Volcanics (GRV) and c. 1585 Ma Benagerie Volcanic Suite in the Curnamona Province (Fig. 1; Daly et al., 1998; Hand et al., 2007; Jagodzinski et al., 2023; Wade et al., 2012). Magmatism at c. 1590 Ma was accompanied by widespread, high temperature metamorphism in the northern and south-eastern Gawler Craton (Cutts et al., 2011; Forbes et al., 2011; Morrissey et al., 2013) and the formation of a diverse range of mineral deposits in the eastern and central Gawler Craton (Fraser et al., 2007; Skirrow et al., 2007). Subsequent events are limited to c. 1520 Ma migmatisation intersected in one drill hole in the northern Gawler Craton (Reid et al., 2014a), minor magmatism at c. 1500 Ma in the southern Gawler Craton (Fanning et al., 2007; Jagodzinski et al., 2006) and localised c. 1450 Ma magmatism, metamorphism and shear zone reactivation in the northern Gawler Craton (Fraser and Lyons, 2006; Morrissey et al., 2019). Biotite Ar–Ar and apatite U–Pb data suggest the Gawler Craton cooled through mid-crustal temperatures by 1400–1300 Ma (Hall et al., 2018; Reid and Forster, 2021; Webb et al., 1986).

2.1. Geology of the Mount Woods Domain

The Mount Woods Domain is a greater than 7000 km^2 geophysically-defined domain in the northern Gawler Craton that is bound by the extension of the Karari Shear Zone to the north and Southern Overthrust to the south (Fig. 2; Betts et al., 2003). Much of the Mount Woods region is poorly outcropping and the geological constraints come from small regions of outcrop augmented by geophysical interpretation and mineral exploration drill holes (Betts et al., 2003; Chalmers, 2007). Recent geophysical interpretation has divided the Mount Woods Domain into three fault-bound zones, the central, southern and western zones (Tiddy

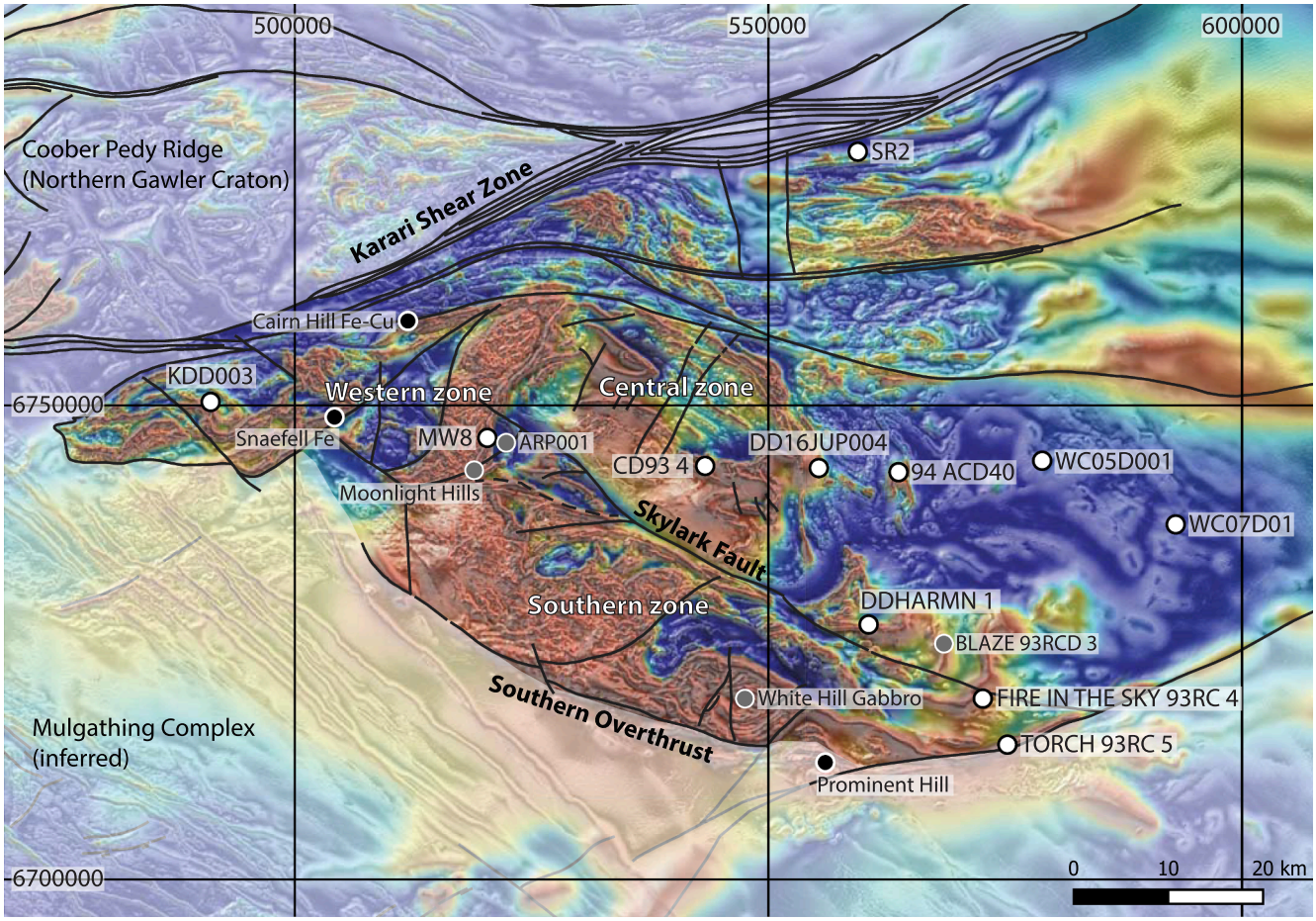

Fig. 2. Total Magnetic Intensity (reduced to pole and reduced to pole tilt) image of the Mount Woods region. White circles denote drill holes used in this study, black circles denote mineral deposits/occurrences and grey circles denote locations of interest mentioned in the text. TMI and shear zone interpretation from South Australian Resources Information Gateway (SARIG; https://map.sarig.sa.gov.au/).

et al., 2020). We broadly adopt this nomenclature, but have redefined the character and spatial extent of each of these zones based on the geological data in this study (as depicted in Fig. 2).

The oldest known rocks in the Mount Woods Domain are granulite facies metasedimentary and intrusive rocks of the Mount Woods Metamorphics in the central zone (Betts et al., 2003; Tiddy et al., 2020). Geochronology from the Mount Woods Metamorphics is limited to a single sample of granulite facies metasedimentary rock intersected in drill hole ARP001 in the western-most part of the central zone (Fig. 2), which yielded a unimodal detrital zircon peak at c. 1860 Ma (Tiddy et al., 2020). The western and southern zone contain interpreted younger sedimentary units, including the c. 1750 Ma Skylark Metasediments, which comprise metapelitic and metapsammitic lithologies, minor banded iron formation and calc silicate (Chalmers, 2007; Jagodzinski et al., 2007; Tiddy et al., 2020). In the southern zone the Skylark Metasediments are unconformably overlain by the Coodnambana Metaconglomerate, which contains a variety of clasts, including pegmatite and metasedimentary rock clasts, interpreted to be derived from the underlying Skylark Metasediments (Chalmers, 2007; Jagodzinski et al., 2007). The depositional age of the Coodnambana Metaconglomerate is poorly constrained between c. 1750 Ma and the timing of upper amphibolite facies metamorphism at 1595 ± 10 Ma (Jagodzinski et al., 2007). There is little published geochronology from intrusive rocks in the Mount Woods Domain. Conventional U–Pb ID-TIMS zircon data from a quartzofeldspathic gneiss yielded an upper intercept of 1742 ± 27 Ma, interpreted to be the timing of magmatic crystallisation (Fanning et al 1988). Mafic and felsic intrusive rocks of the Balta Granite Suite, which is equivalent to the Hiltaba Suite, have been identified in drill core and outcrop in the southern and western zones and give SHRIMP U–Pb ages of 1586.8 ± 4.1 Ma and 1586.3 ± 2.8 Ma (Jagodzinski, 2005). Other intrusive ages that have previously been quoted in the literature are a granite intersected in drill hole in the eastern Mount Woods region with a magmatic age of 1708 ± 3 Ma (Holm, 2004), the 1691 ± 25 Ma Engenina Adamellite in the southern zone and the c. 1562 Ma White Hill Gabbro Complex (Allen et al., 2016). However, these ages come from unpublished honours theses or conference abstracts that do not provide the data or concordia plots, making it difficult to assess the reliability of the ages.

The Mount Woods Domain records multiple phases of deformation and metamorphism, though the overall metamorphic history is not well understood. In the central zone, Betts et al. (2003) interpreted that a layer-parallel gneissic foliation and isoclinal folds were associated with granulite facies metamorphism at c. 1730 Ma, followed by emplacement of the c. 1692 Ma Engenina Adamellite and the formation of open to isoclinal folds. However, there is currently no published metamorphic age data to support c. 1730–1690 Ma Kimban-aged metamorphism in the Mount Woods Domain. The inference of Kimban-aged structures is predominantly based on cross-cutting relationships in the regional geophysics (Tiddy et al., 2020) and the presence of gneissic clasts and xenoliths in the Coodnambana Metaconglomerate and Engenina Adamellite, respectively (Betts et al., 2003; Chalmers, 2007).

Metamorphic zircon rims from the Coodnambana Metaconglomerate south of the Skylark Fault give an age of 1595 ± 10 Ma (Jagodzinski et al., 2007). Granitic gneiss with a protolith age of 1586.3 ± 2.8 Ma (Jagodzinski, 2005) places an upper bound on the age of high-grade deformation in the southern zone. Monazite CHIME chemical U–Th–Pb ages of c. 1615 Ma were interpreted to reflect monazite growth during prograde metamorphism, whereas peak metamorphism was interpreted to be coeval with c. 1590–1570 Ma magmatism (Forbes et al., 2011). Metamorphic conditions during this event reached 4.7 kbar and ~ 750 °C, with a high thermal gradient prograde history that involved andalusite (Forbes et al., 2011). Most recently, Tiddy et al. (2020) proposed that the Mount Woods Domain was a metamorphic core complex at c. 1600–1580 Ma that was modified by shear zone reactivation during the c. 1570–1540 Ma Kararan Orogeny. Geophysical interpretation of fault zones in the northern Mount Woods region are thought to reflect a phase of NE–SW shortening that exhumed the Mount Woods Domain (Tiddy et al., 2020). Two biotite ^{40}Ar–^{39}Ar ages of 1565 ± 11 and 1557 ± 11 Ma from drill hole ARP001 are interpreted to reflect that the central zone cooled 20 Myr earlier than the southern zone, which records biotite ^{40}Ar–^{39}Ar ages of 1540 ± 8 Ma and 1539 ± 8 Ma from two locations (Moonlight Hills and drill hole BLAZE 93RCD 3, Fig. 2; Forbes et al., 2012; Tiddy et al., 2020). Apatite U–Pb ages of c. 1540–1400 Ma from Balta Suite granites are broadly consistent with cooling through this interval (Hall et al., 2018).

3. Sample selection and methods

Samples were taken from across the Mount Woods Domain to investigate whether the three fault-bound zones record different geological histories (Fig. 2). There is very little outcrop, so sampling is mostly limited to mineral exploration drill holes that intersect basement. The use of drill core limits the available sample size, requiring that in some cases slightly different intervals were used for geochronology and phase equilibria modelling. The samples in this study were analysed as part of several distinct projects over a four-year period, hence there is some variation in the duration of analysis and the elements/isotopes measured.

3.1. U–Pb zircon and monazite geochronology

LA–ICP–MS zircon geochronology was done on five samples from four drill holes (Table 1). Four samples (2673257, 2673258, 2345928 and 2449516) yielded detrital zircon with little to no analysable metamorphic zircon and were used to constrain the depositional age of the sedimentary protoliths, whereas one sample (2490081) only yielded metamorphic zircon. LA–ICP–MS monazite geochronology was done on 11 samples from 10 drill holes and one outcrop sample, with samples 2345928, 2490081 and 2673257 done in grain mount and the remaining samples analysed in situ in thin sections (Table 1). Monazite and zircon for grain mounts were separated using a combination of panning, heavy liquids, magnetic separation and hand picking to obtain a clean separate. Grains were then mounted in epoxy resin, polished to half grain thickness and photographed using transmitted and reflected light on an optical microscope. Mounted monazite and zircon grains were imaged using a back-scattered electron (BSE) detector on a FEI Quanta 600 Scanning Electron Microscope (SEM) at Adelaide Microscopy, with zircons also imaged using a Gatan Cathodoluminescence (CL) detector attached to the same SEM. Analysis spots for zircon were selected based on CL and transmitted light images with the aim of targeting all domains identified in CL images and avoiding visible cracks or inclusions. In situ monazites were first located in each thin section using Mineral Liberation Analysis (MLA) software on the FEI Quanta 600 SEM. Selected grains were then imaged using a BSE detector on a Phillips XL30 SEM to characterise the microstructural location and compositional variability.

Zircon and monazite grains were analysed using a RESOlution LR 193 nm Excimer laser in a He ablation atmosphere coupled to an Agilent 7900x ICP–MS. Ablation was performed with a frequency of 5 Hz and spot sizes of 19– 29 μm for zircon and 9–19 μm for monazite, depending on grain size. Data acquisition included 30–50 s of background measurement and 30–50 s of ablation, depending on grain size. Trace elements were collected for some samples to assist with signal selection and interpretation. A list of the measured masses and parameters used for each sample are provided in Appendix 1.

Zircon and monazite isotopic data were reduced using Iolite v 3 software (Paton et al., 2011; Paton et al., 2010). Elemental fractionation and mass bias for zircon geochronology were corrected using the primary zircon standard GJ-1 (TIMS data: $^{207}Pb/^{206}Pb = 607.7 \pm 4.3$ Ma, $^{206}Pb/^{238}U = 600.7 \pm 1.1$ Ma and $^{207}Pb/^{235}U = 602.0 \pm 1.0$; Jackson et al., 2004) with standards bracketing every 10–15 unknown zircon analyses. Data accuracy was monitored using secondary zircon standards Plešovice (TIMS data: $^{206}Pb/^{238}U = 337.13 \pm 0.37$ Ma; Sláma

Table 1
Summary of studied samples.

Sample	Drill hole no.	Drill hole name	Zone	Easting (GDA 2020)	Northing	Meterage (m)	Dominant mineralogy	Zr U–Pb age ± 2σ (Ma)	Mnz U–Pb age ± 2σ (Ma)	Bt Rb–Sr age ± 2σ (Ma)
Central zone										
2449518	189193	Fire in the Sky 93RC 4	53	572,630	6,719,073	90.00–111.00	pl + kfs + qz + grt + bt (+ms)	–	c. 2470 1702 ± 4	–
2673257	235676	WC07D01	53	593,001	6,737,452	1126.5–1126.7	bt + kfs + pl + qz + sil + crn (+po)	< 2550 (max. dep.)	1695 ± 7	1475 ± 61
2673258	235676	WC07D01	53	593,001	6,737,452	1127.5–1127.65	kfs + grt + crd + qz + pl + bt + sil + crn + spn + ilm + po (+ms)	< 2550 (max. dep.)	–	1464 ± 45
2490078	210004	WC05D001	53	578,901	6,744,172	818.38–819.20	grt + kfs + qz + sil + crd + bt + ilm + mag	–	c. 1694	1389 ± 30
2449517	189411	94ACD 40	53	563,730	6,742,967	69.25–70.00	bt + sil + qz + crd + kfs + pl + mag (+ms + chl)	–	1701 ± 5	1425 ± 55
2345928	185584	CD93 4	53	543,309	6,743,625	175.85–176.65	qz + bt + grt + kfs + pl ± crd (+ms)	1855 ± 5 (max. dep.)	1692 ± 5 1675 ± 5	1484 ± 49
2345929	185584	CD93 4	53	543,309	6,743,625	179.85–180.05	qz + kfs + pl + bt + grt + crd (+ms + chl)	–	–	1437 ± 61
2673261	294587	DD16JUP004	53	555,313	6,743,404	303.00–303.25	grt + kfs + pl + crd + bt + spn + crn + qz + ilm + po	–	1702 ± 5	1470 ± 23
Western zone										
2490081	215243	KDD003	53	491,201	6,750,251	222.40–223.35	grt + qz + crd + kfs + sil + bt + spn + ilm + po	1677 ± 12 (metm.)	1694 ± 6 1568 ± 16 c. 1515	1394 ± 44
MW8	–	Outcrop	53	519,360	6,743,439	–	qz + grt + bt + kfs + pl + crd + spn + sil + ilm	–	1672–1534	–
Adjacent to shear zones; Central, Southern and Northern Mount Woods Domain										
2332807	188525	DDHARMN 1	53	560,574	6,726,890	258.35–258.60	qz + pl + bi + ksp + sil + mag + grt	–	1683 ± 13 1549 ± 18	1453 ± 29
2332809	188525	DDHARMN 1	53	560,574	6,726,890	136.10–136.40	qz + bi + ksp + pl + sil + grt + mag	–	–	1425 ± 27
2449515	189194	TORCH 93RC 5	53	575,230	6,714,223	156.80–157.50	kfs + qz + pl + bt + ms + mag	–	1567 ± 8	
2449516	189194	TORCH 93RC 5	53	575,230	6,714,223	159.40–160.35	kfs + qz + pl + bt + ms + mag	1755 ± 9 (max dep.)	–	1442 ± 21
2345927	138089	SR2	53	559,430	6,776,773	129.05–129.40	qz + kfs + crd + sil + grt + bt + pl + ilm	–	1613–1478	1455 ± 30

Ages given are $^{207}Pb/^{206}Pb$. Abbreviations from Whitney and Evans (2010). Biotite (bi), chlorite (chl), cordierite (crd), corundum (crn), garnet (grt), ilmenite (ilm), K-feldspar (kfs), magnetite (mag), muscovite (ms), plagioclase (pl), pyrrhotite (po), quartz (qz), sillimanite (sil), spinel (spn). Minerals in brackets are interpreted to be the product of retrogression/alteration.

et al., 2008) and 91,500 (TIMS data: $^{207}Pb/^{206}Pb = 1065 \pm 0.4$ Ma; Wiedenbeck et al., 1995). The weighted mean ages of external standards analysed over the course of this study were as follows: Plešovice: $^{206}Pb/^{238}U = 340 \pm 0.60$ Ma ($n = 58/59$, MSWD = 1.9), and 91500: $^{207}Pb/^{206}Pb = 1060 \pm 7$ Ma ($n = 52$, MSWD = 0.98). Elemental fractionation and mass bias for monazite geochronology was corrected using the primary standard MAdel (TIMS data: $^{207}Pb/^{206}Pb = 492.01 \pm 0.77$ Ma, $^{206}Pb/^{238}U = 517.9 \pm 2.6$ Ma and $^{207}Pb/^{235}U = 513.13 \pm 0.20$ Ma updated from Payne et al. (2008) with additional TIMS analyses), with standard bracketing every 10–15 unknown analyses. Data accuracy was monitored using the in-house monazite standard 94–222/Bruna-NW (SHRIMP data: $^{206}Pb/^{238}U = 450.2 \pm 3.4$ Ma; Maidment, 2005). Over the course of the study, 54 analyses of 94–222 yielded weighted mean ages of $^{206}Pb/^{238}U = 447.52 \pm 0.99$ (MSWD = 1.09). Uncertainties on weighted mean ages are presented at 95 % confidence. Where trace elements were collected, zircon analyses were assumed to contain stochiometric Zr contents (43.14 wt%). All monazite analyses were assumed to have 20 wt% Ce.

3.2. Rb–Sr biotite geochronology

In situ Rb–Sr data were collected on sample thin sections in the GeoHistory Facility, JdLC, Curtin University, across three sessions. For all sessions, a RESOlution LR 193 nm ArF excimer laser with a Laurin Technic S155 sample cell and Squid smoothing device was used. Laser settings comprised a beam diameter of 64 μm, an on-sample energy of 2.5 J cm^{-2}, a repetition rate of 5 Hz, 60 s of analysis time and 30 s of on-peak background acquisition with the laser off. All analyses were preceded by two cleaning pulses. The sample cell was flushed with ultrahigh-purity He (320 mL min^{-1}) with added N2 (1.2 mL min^{-1}), both of which were passed through an inline Hg trap.

Rb–Sr data were collected on an Agilent 8900 triple quadrupole mass spectrometer in MS/MS mode using N_2O reaction gas following the method of Olierook et al. (2020). The reaction cell was flushed with N_2O for several hours before sample analysis to ensure signal stability. NIST610 was used to tune N_2O to maximize intensity at mass 104 ($^{88}Sr^{16}O$), while maintaining less than 7 cps at mass 101 ($^{85}Rb^{16}O$).

The analytical protocol is designed so as to stay below the P/A (Pulse/Analogue) conversion thresholds for Rb and Sr. This is achieved by assessing the daily sensitivity conditions of the ICP-MS and reducing the ablation spot size as needed to ensure all standard and sample signals are analysed in Pulse detector mode. Instrument conditions were sufficiently consistent over the course of this study such that all analyses were conducted with a single spot size of 64 μm. $^{87}Sr/^{86}Sr$ and $^{87}Rb/^{86}Sr$ are initially externally calibrated against NIST610 using certified values of $^{87}Sr/^{86}Sr = 0.709699 \pm 0.000018$ and 2.390 ± 0.005 (Woodhead and Hergt, 2001). This calibration is done using Iolite (Paton et al., 2011; Paton et al., 2010) and accounts for fundamental instrument drift within each run. The measured $^{87}Sr/^{86}Sr$ result for the plagioclase MIR a in this study is 0.7049 ± 0.0041 which is within uncertainty of the published isotopic composition of 0.70310 ± 0.00007 (Rankenburg et al., 2004). The measured $^{87}Sr/^{86}Sr$ for pressed powder tablets of phlogopite Mica-Mg calibrated against NIST610 for the three analytical sessions within this study were 1.847 ± 0.011 (95% CI, $n = 25$, MSWD = 0.66), $1.846 \pm$

0.023 (95% CI, $n = 12$, MSWD = 1.4) and 1.849 ± 0.018 (95% CI, $n = 23$, MSWD = 2.0). These values are calculated using internal uncertainties from the analyses plus an additional 2.5% uncertainty which reflects the long-term additional uncertainty for the method at the time of analyses in the laboratory. Additional spread in part reflects heterogeneity within the MicaMg standard and variability of ablation characteristics (Redaa et al., 2021). As a result of this heterogeneity, sample-standard bracketing using a subset of Mica-Mg analyses for each block within the runs has the potential to result in erroneous corrections for a given analysis. To minimise the effects of this heterogeneity, a single post-Iolite processing correction was applied to the $^{87}Rb/^{86}Sr$ values of the samples in each session using an average correction obtained from the Mica-Mg analyses within each run. The correction values were determined by determining the necessary correction to obtain the known crystallisation age of Mica-Mg (519.4 ± 6.5 Ma (2σ); Kröner et al., 1996) using an initial $^{87}Sr/^{86}Sr$ of 0.72607 ± 0.00070 (Hogmalm et al., 2017) and the data from each session. This approach allows for the natural variation in $^{87}Rb/^{86}Sr$ ratios of Mica-Mg to be counteracted by the subsequent variation in the measured, present day $^{87}Sr/^{86}Sr$ ratios. This produces $^{87}Rb/^{86}Sr$ normalisation factors of 0.8969, 0.8921 and 0.9066. Uncertainties associated with the NIST610 and Mica-Mg normalisations are propagated in quadrature on the unknowns as per Olierook et al. (2020). Rb–Sr isochrons and ages were computed using IsoplotR (Vermeesch, 2018). All uncertainties provided in the text are presented at 95 % confidence. Full isotopic data for the samples and reference materials are given in Appendix 1.

3.3. Phase equilibria modelling

Samples selected for phase equilibria forward modelling came from relatively homogenous intervals of drill core and avoided domains of coarse-grained minerals or large leucosomes that were not representative of the overall rock volume. Whole rock geochemical data for phase equilibria modelling were determined by Bureau Veritas, Perth. Samples were powdered and fused with 4% Li nitrate to form a glass bead. Major elements were determined by X-ray fluorescence spectrometry and trace elements were analysed by Laser Ablation Mass Spectrometry. FeO was determined by volumetric titration. Whole rock geochemistry is presented in Appendix 2.

Phase equilibria models for two samples were calculated using THERMOCALC v3.40, using the internally consistent dataset, ds62, of Holland and Powell (2011) and the activity–composition (a–x) models re-parameterised for metapelitic rocks in the system MnNCKFMASHTO ($MnO–Na_2O–CaO–K_2O–FeO–MgO–Al_2O_3–SiO_2–H_2O–TiO_2–Fe_2O_3$) (Powell et al., 2014; White et al., 2014a; White et al., 2014b). Fe_2O_3 was determined by titration, and the sensitivity of the peak assemblage to variations in oxidation state was assessed using T–M_O sections. The T–M_O sections highlight that the modelled peak conditions are not sensitive to small variations in oxidation state (Appendix 3). The measured LOI may only provide a maximum value for the amount of H_2O at peak conditions due the presence of other volatiles such as CO_2, F and Cl and evidence for alteration of cordierite and feldspar in some samples. The H_2O contents for each sample were determined using the modal proportion of hydrous minerals (biotite and cordierite). The sensitivity of the modelled peak conditions to H_2O content were assessed using T–M_{H2O} sections, presented in Appendix 3.

4. Results: Geochronology

A summary of each sample is provided below, with detailed petrography and sample descriptions provided in Appendix 4. Only those analyses that are within 2σ uncertainty of concordia are used for the calculation of weighted average ages and probability density plots. Discordant analyses that fall within the window of the concordia plot are shown as grey dashed ellipses. Uncertainties on weighted average ages are quoted using 95% confidence. Where trace elements were collected they are mentioned in the text, with representative plots presented in Appendix 5. Rb–Sr isochrons are presented in Appendix 6.

4.1. Central zone

4.1.1. Sample 2449518 (Fire in the Sky)

Sample 2449518 is composed of ~1 × 0.5 cm drill chips that are dominated by coarse-grained K-feldspar, quartz and plagioclase. Some chips contain euhedral garnet and rare, tabular biotite (Fig. 3a). It is not possible to determine whether the sample is foliated from the mineralogical texture of the small drill chips, however, the rock is likely to be a granite or granitic gneiss.

Forty-four analyses were collected from 16 monazite grains mounted in epoxy resin. Monazite grains are typically 100–200 μm in diameter and display patchy core–rim zoning in BSE. A Tera–Wasserburg plot of all analyses defines a discordia with an upper intercept of 2471 ± 21 Ma and a lower intercept of 1663 ± 11 Ma (Fig. 4a; $n = 44$, MSWD = 1.13). A weighted mean age of the concordant analyses defining the younger population is 1702 ± 4 Ma ($n = 31$, MSWD = 0.45), which is taken to be the age of metamorphism. There is no relationship between age and grain size, BSE response or trace element character.

No biotite Rb–Sr data was collected from this sample due to the paucity of biotite. This sample is interpreted to be an early Paleoproterozoic aluminous granite that was metamorphosed at c. 1700 Ma, similar to rocks elsewhere in the central Mount Woods Domain (Fig. 4b).

4.1.2. Samples 2673257 and 2673258 (WC07D01)

Sample 2673257 is a biotite-rich gneiss containing patches of acicular sillimanite and corundum (Fig. 3b). Sample 2673258 is biotite-poor, weakly foliated and contains abundant coarse-grained garnet, cordierite and magnetite. Samples 2673257 and 2673258 were used for detrital zircon geochronology, whereas monazite geochronology was only collected from sample 2673257.

Zircon grains in sample 2673257 are 75–150 μm in length with aspect ratios of 1:1 to 1:2 and rounded terminations (Fig. 5a). In CL images they commonly display strongly to weakly oscillatory zoned cores that are overgrown by narrow, discontinuous rims with a low CL response that were mostly too thin to analyse. Other grains are dark with patchy zoning and are interpreted to be metamict. Seventy-eight analyses were collected from 73 grains mounted in epoxy resin, of which 15 were concordant. Concordant analyses range in age from 2827 to 1724 Ma, with a dominant age peak at 2684 Ma ($n = 11$) and single ages at 2827 Ma, 2370 Ma, 2283 Ma and 1724 Ma. The youngest analysis (1724 ± 37 Ma) comes from a rim domain and has a low Th/U ratio of 0.07, a flat HREE pattern, and is interpreted to be metamorphic. The remaining concordant analyses come from zoned core domains, have Th/U ratios of 0.38–1.49 and are interpreted to be detrital. The small number of concordant analyses and high amounts of Pb loss make it difficult to determine the maximum depositional age. The two young analyses with ages of c. 2400–2200 Ma plot within the discordant array and are interpreted to have experienced Pb loss. In addition, there are no significant tectonic events in the 2400–2200 Ma interval in the Gawler Craton that are likely to provide a source for detrital zircon of this age (Belousova et al., 2009). Therefore, more conservatively, the maximum age of deposition is likely to be c. 2550 Ma.

Zircon grains in sample 2673258 are similar in size and appearance to those in sample 2673257 (Fig. 5b). They are typically oscillatory zoned with highly variable CL response between grains. Rare grains display narrow, dark rims that were too thin to analyse. Seventy-four analyses were collected from 73 grains mounted in epoxy resin. The majority of analyses are moderately to highly discordant. The 28 concordant analyses come from oscillatory zoned cores and have $^{207}Pb/^{206}Pb$ spot ages between 2816 and 2528 Ma and Th/U ratios of 0.35 to 1.22. A probability density plot broadly defines two peaks at ~ 2715 Ma and 2640 Ma. The three youngest analyses have ages between 2552 and 2528 and come from strongly oscillatory zoned grains,

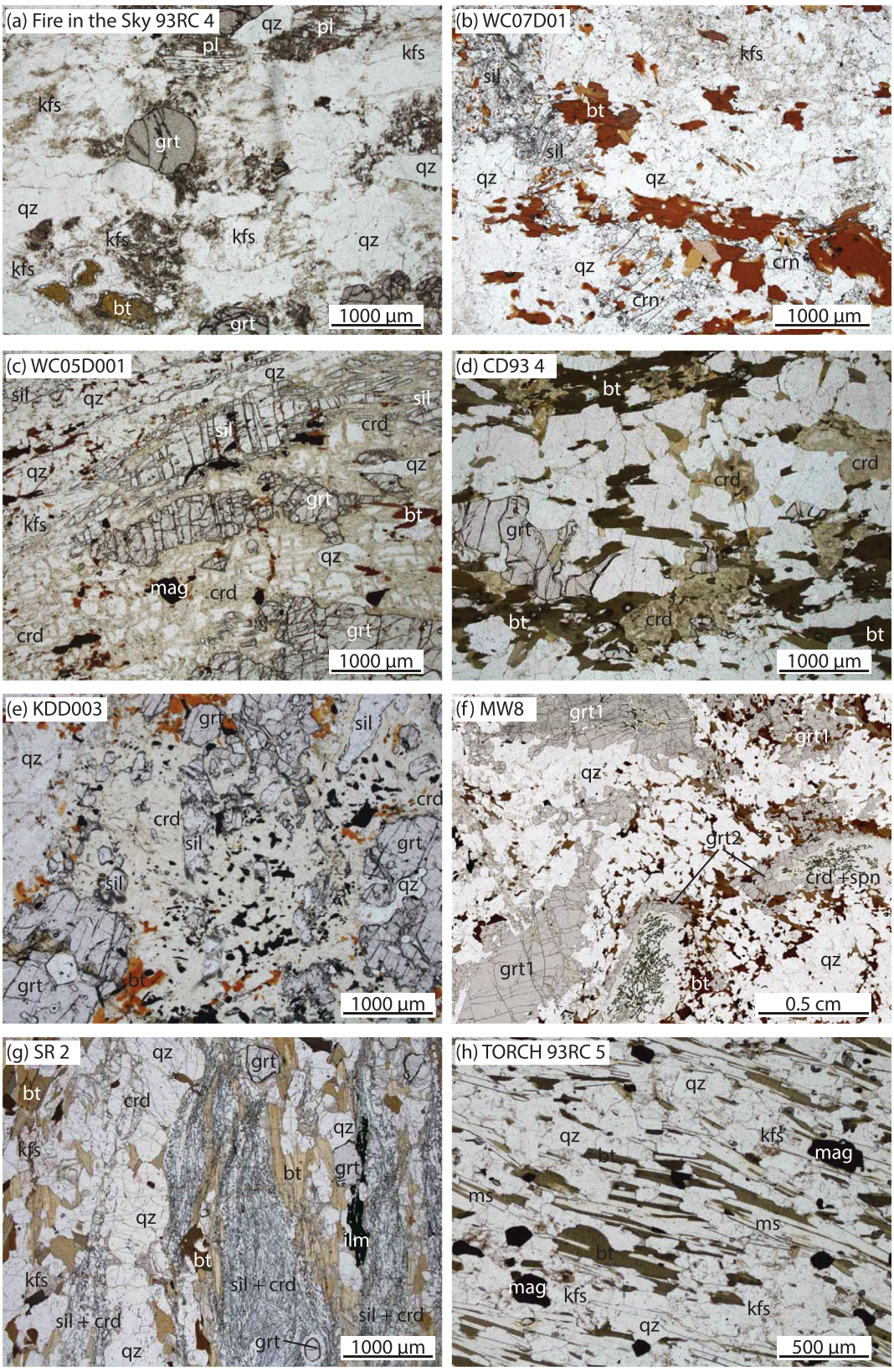

Fig. 3. Representative photomicrographs of samples used in this study. (a) Garnet-bearing granite from drill hole Fire in the Sky. (b) Aluminous metasedimentary rock containing sillimanite and corundum from drill hole WCD007. (c) Coarse-grained garnet and sillimanite separated by partially altered cordierite from drill hole WC05D001. (d) Garnet–cordierite–biotite gneiss from drill hole CD93 4. (e) Coarse-grained garnet and sillimanite surrounded by symplectitic coronas of cordierite, spinel and ilmenite from drill hole KDD002. (f) Cordierite–spinel symplectites surrounded by coronas of garnet from outcrop sample MW8. (g) Strongly foliated garnet–sillimanite–cordierite gneiss from drill hole SR 2. Sillimanite only occurs as inclusions in cordierite. (h) Muscovite–biotite–K-feldspar schist from drill hole TORCH 93 RC 5.

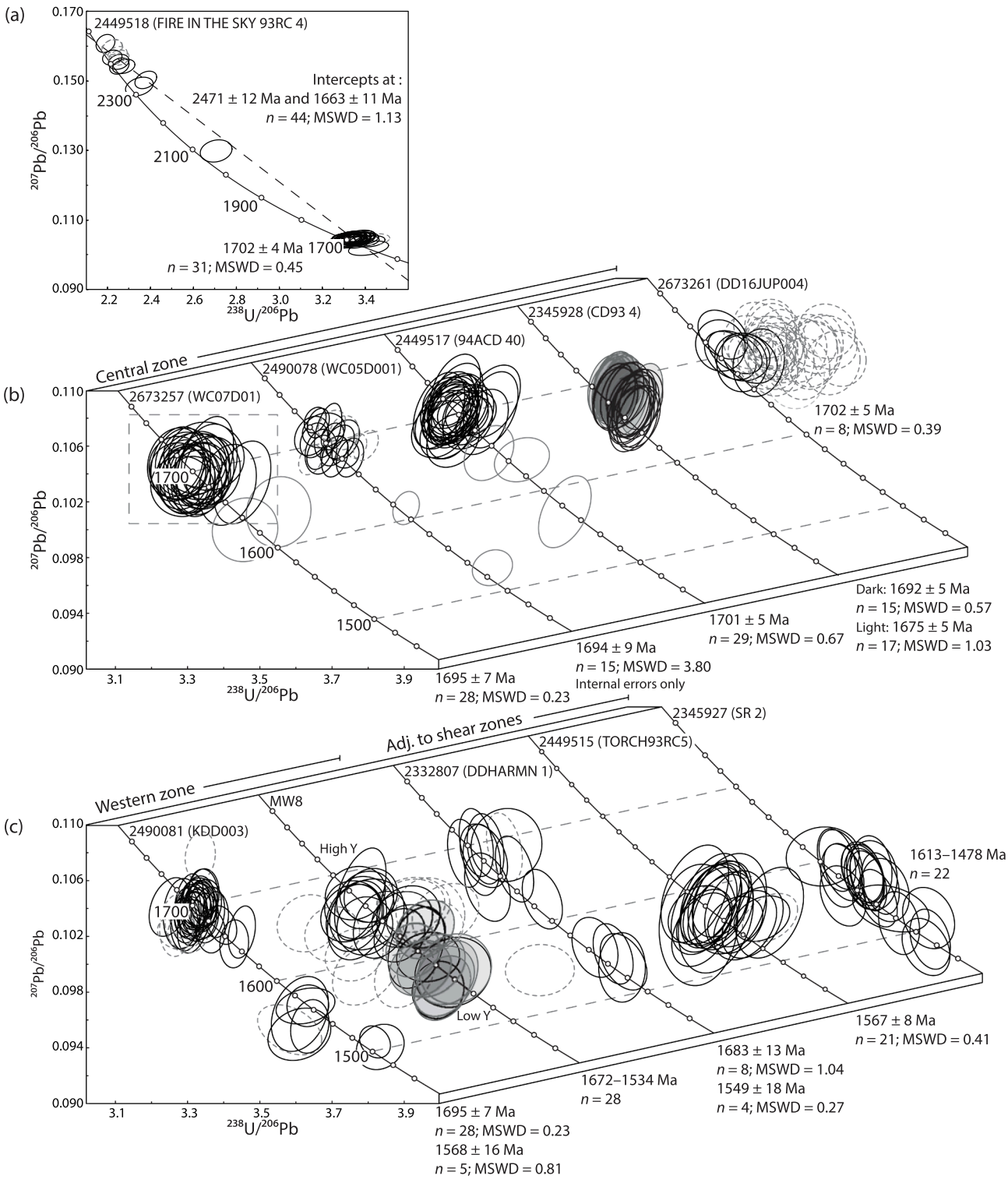

Fig. 4. Monazite geochronology data. All ages are $^{207}Pb/^{206}Pb$ ages. All data-point error ellipses on the stacked Tera–Wasserburg concordia plots are 2σ. Concordant analyses that are not included in the calculation of weighted mean ages are shown as grey ellipses; discordant analyses are shown as dashed ellipses. (a) Sample 2449518 from drill hole Fire in the Sky 98 RC 4; (b) Eastern-Central Mount Woods Domain. samples 2673257 (WC07D01), 2490078 (WC05D001), 2449517 (94ACD40), 2345928 (CD93 4), 2673261 (DD16JUP004), (c) Western-Central Mount Woods Domain. samples 2490081 (KDD003), MW8; and samples adjacent to shear zones. 2332807 (DDHARMN 1), 2449515 (TORCH 93RC 5), 2345927 (SR 2).

suggesting the maximum depositional age is younger than 2550 Ma.

Monazite grains separated from sample 2673257 are rounded to elongate, 50–110 μm in diameter and display patchy zoning in BSE images. Rare grains show a dark core that is typically high in HREE, surrounded by discontinuous, brighter rims. Thirty analyses were collected from 17 grains. Individual $^{207}Pb/^{206}Pb$ ages range from 1710 to 1620 Ma, with no relationship between BSE zoning and age (Fig. 4b). The $^{207}Pb/^{206}Pb$ weighted mean age of the oldest 28 analyses is 1695 ± 7 Ma (MSWD = 0.23, prob. = 1.0). There is a broad change in monazite trace element composition of the main population with time, with the

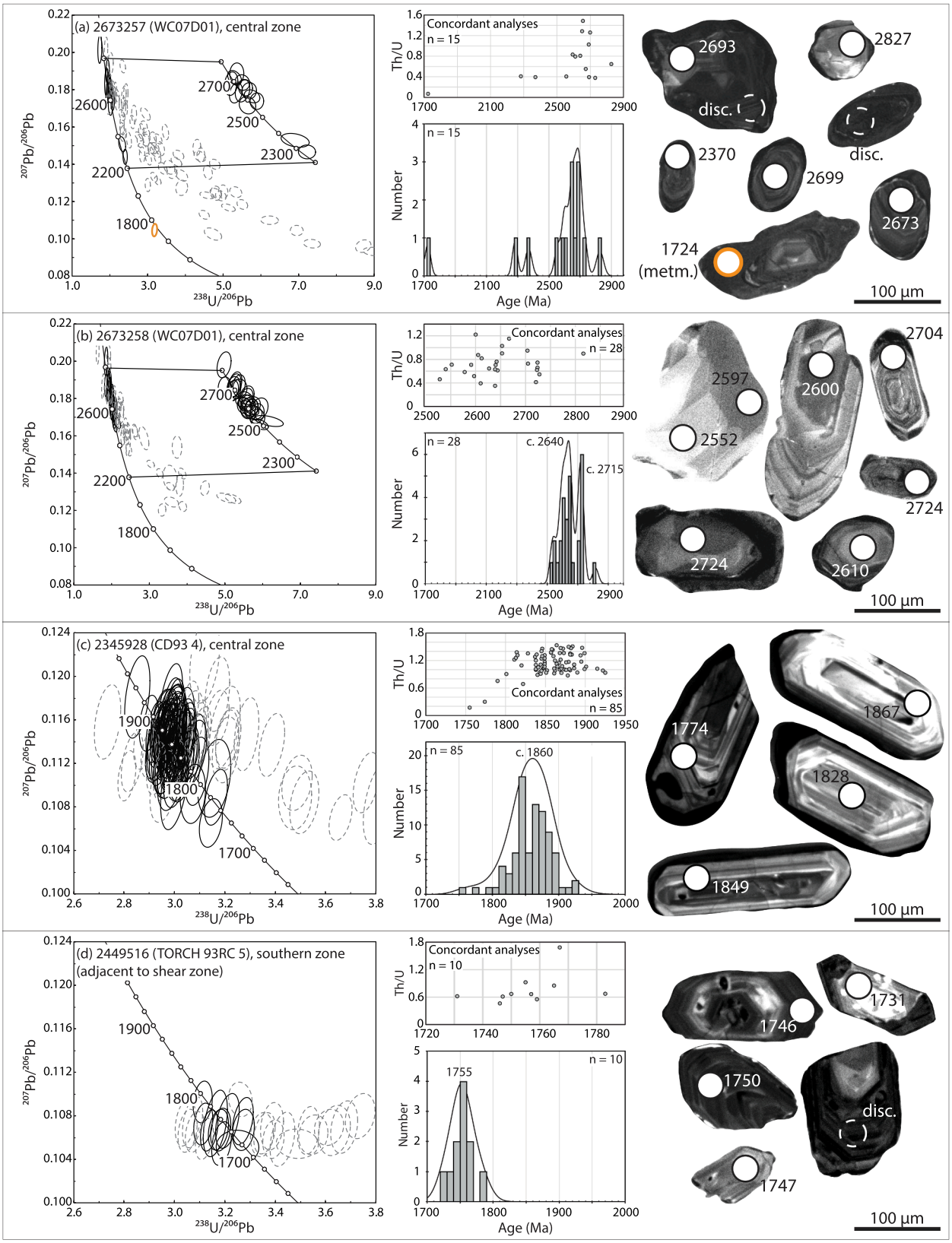

Fig. 5. Detrital zircon geochronology data. All ages given on CL images and probability density plots are $^{207}Pb/^{206}Pb$ ages. All data-point error ellipses on the concordia plots are 2σ. Discordant analyses are shown as dashed ellipses. (a) Sample 2673257, drill hole WC07D01. A single analysis of a metamorphic rim is highlighted by the orange outline. (b) Sample 2673258, drill hole WC07D01. (c) Sample 2345928, drill hole CD93 4. (d) Sample 2449516, drill hole TORCH 93RC 5. (For interpretation of the references to colour in this figure legend, the reader is referred to the web version of this article.)

oldest analyses having shallower Eu anomalies and higher HREE contents than the younger analyses but the ages of each compositional group are within uncertainty (Appendix 5). The two youngest analyses have ages of 1638 ± 38 Ma and 1620 ± 39 Ma and are interpreted to have experienced Pb loss.

Forty-seven analyses from foliated biotite in sample 2673257 give an isochron age of 1475 ± 61 (MSWD = 0.87), whereas 28 analyses of platy biotite from sample 2673258 give an isochron age of 1464 ± 45 (MSWD = 0.72).

In summary, drill hole WC07D01 contains an interlayered sedimentary sequence that was likely deposited after 2550 Ma and predominantly contains Archean detritus with ages between 2640 and 2720 Ma. Metamorphic monazite suggests the metasedimentary rocks were metamorphosed at 1695 ± 7 Ma, which is within uncertainty of the age of a single interpreted metamorphic zircon rim at 1724 ± 37 Ma.

4.1.3. Sample 2490078 (WC05D001)

Sample 2490078 is a gneiss with a strong foliation defined by sillimanite, elongate garnet and stromatic quartzofeldspathic leucosomes. Garnet grains are separated from sillimanite by moats of partially altered cordierite (Fig. 3c).

Monazite from sample 2490078 is equant to elongate, 20–40 μm in diameter and displays patchy zoning in BSE images. Elongate grains are parallel to the foliation. Twenty-three analyses were collected in situ from 10 grains located along grain boundaries in the foliated matrix. Six analyses were excluded on the basis of discordance. The remaining analyses yield a main population with a poorly defined $^{207}Pb/^{206}Pb$ weighted average age of 1694 ± 9 (n = 15, MSWD = 3.8, prob. = 0). Two concordant analyses at 1604 ± 18 Ma and 1526 ± 20 Ma are statistical outliers from the main population (Fig. 4b).

Fifty analyses of biotite were collected from three textures: foliated biotite in the leucosomes, a single grain included in garnet and anhedral platy biotite at the margins of cordierite. All analyses give an isochron age of 1389 ± 30 Ma (MSWD = 0.52).

4.1.4. Sample 2449517 (94ACD 40)

Sample 2449517 is a strongly foliated metapelitic gneiss containing biotite, sillimanite, altered cordierite and quartzofeldspathic leucosomes. The sample has been partially retrogressed, with partial replacement of feldspars by muscovite and minor replacement of biotite by muscovite and chlorite.

Monazite grains in this sample are 150–250 μm in diameter. Some grains show clear core–rim textures in BSE images, whereas others contain very bright, irregular zones. Thirty-two analyses were collected from 10 grains mounted in epoxy resin. Three anomalously young analyses were excluded from the calculation of a weighted mean age. The 29 oldest analyses yield a $^{207}Pb/^{206}Pb$ weighted average age of 1701 ± 5 Ma (Fig. 4b; MSWD = 0.67, prob. = 0.90). The three excluded younger analyses come from bright domains and give ages between c. 1650–1570 Ma. However, not all bright domains yield young ages and those grains with clear core–rim textures do not show any age difference between zones.

Twenty-six analyses of euhedral foliated biotite from sample 2449517 give an isochron age of 1425 ± 55 Ma (MSWD = 0.5).

4.1.5. Samples 2345928 and 2345929 (CD93 4)

Two samples were selected from drill hole CD93 4 from intervals less than 3 m apart. The samples are gneissic, contain quartzofeldspathic leucosomes and form part of an interlayered pelitic–psammitic metasedimentary sequence. Sample 2345928 is dominantly comprised of biotite and quartz, with lesser K-feldspar, altered plagioclase and aggregates of skeletal garnet. Sample 2345928 was crushed for zircon and monazite geochronology. Sample 2345929 contains garnet, biotite, quartz, coarse-grained K-feldspar, minor altered plagioclase and domains of intergrown sericite and pinnite that are interpreted to be altered cordierite (Fig. 3d). Sample 2345929 was used for phase equilibria modelling.

Zircon grains in sample 2345928 are typically 200–400 μm in length with aspect ratios greater than 1:3 and rounded to prismatic terminations. All zircons display oscillatory zoning in CL (Fig. 5c). Many of the zircon grains have low CL response rims (≪20 μm) that are too thin to be analysed. 122 oscillatory zoned cores were analysed from 122 grains mounted in epoxy resin. All analysed cores are interpreted to be detrital. Thirty-seven analyses were excluded from further interpretation on the basis of concordance. The remaining 85 analyses range in age between 1925 and 1755 Ma (Fig. 5c). The Th/U ratios of all concordant analyses range between 0.69 and 1.53, with the exception of the two youngest grains (1774 ± 36 Ma and 1755 ± 32 Ma) which have Th/U ratios of 0.30 and 0.17, respectively (Fig. 5c). These young grains with low Th/U ratios may reflect partial Pb loss during granulite facies metamorphism (below) and are not considered further. A conservative maximum depositional age for this sample is given by a $^{207}Pb/^{206}Pb$ weighted mean age of 1855 ± 5 Ma (MSWD = 1.3, prob. = 0.056). The zircon geochronology does not provide any constraints on the age of metamorphism.

Monazite grains are 100–450 μm, rounded and display patchy zoning in BSE images. Thirty-two analyses were collected from seven grains mounted in epoxy resin. The $^{207}Pb/^{206}Pb$ weighted average age of all 32 analyses is 1683 ± 4 Ma (Fig. 4b; MSWD = 1.5, prob. = 0.034). There is a generalised relationship between monazite zoning and age, with darker zones typically yielding older ages. The $^{207}Pb/^{206}Pb$ age of 15 analyses from the dark zones is 1692 ± 5 Ma (MSWD = 0.57, prob. = 0.89) whereas the $^{207}Pb/^{206}Pb$ age of analyses from the bright zones is 1675 ± 5 Ma (n = 17, MSWD = 1.03, prob. = 0.42).

Twenty-six analyses of foliated biotite from sample 2345928 give an isochron age of 1484 ± 49 Ma (MSWD = 0.84), whereas 25 analyses from sample 2345929 give an isochron age of 1437 ± 61 Ma (MSWD = 1.6).

In summary, drill hole CD93 4 contains an interlayered metapelitic–psammitic sequence that was deposited after 1855 ± 5 Ma. This inferred sedimentary sequence was metamorphosed and partially melted between c. 1690–1675 Ma.

4.1.6. Sample 2673261 (DD16JUP004)

Sample 2673261 contains coarse-grained garnet, cordierite, feldspar (perthite, antiperthite and plagioclase) and lesser biotite and quartz. Cordierite-rich domains contain symplectites of anhedral corundum, spinel, ilmenite and pyrrhotite.

Monazite grains are 30–100 μm in diameter and unzoned in BSE images. Monazite occurs as inclusions in coarse-grained garnet, biotite and cordierite, adjacent to fine-grained biotite zones, and along grain boundaries within the corundum-bearing symplectites. Thirty-seven analyses were collected from 16 grains. The majority of monazite analyses show evidence for recent Pb loss leading to minor discordance (Fig. 4b). Eight concordant analyses give a $^{207}Pb/^{206}Pb$ weighted average age of 1702 ± 5 Ma (MSWD = 0.39, prob. 0.91). A weighted mean of all analyses gives an indistinguishable $^{207}Pb/^{206}Pb$ weighted average age of 1699 ± 3 Ma (n = 36/37; MSWD = 1.04, prob. = 0.41). There is no link between microstructural location or trace element character and age.

Forty-one analyses of weakly foliated biotite from sample 2673261 give an isochron age of 1470 ± 23 Ma (MSWD = 1.6).

4.2. Western zone

4.2.1. Sample 2490081 (KDD003)

This sample is a garnet-rich gneiss containing a foliation defined by quartzo-feldspathic leucosomes. Garnet and rare sillimanite are separated by moats of cordierite (mostly altered to pinnite) containing ilmenite, pyrrhotite, quartz, biotite and rare spinel (Fig. 3e). Sample 2490081 was used for zircon and monazite geochronology.

Zircon grains are rounded and 100–130 μm in diameter (Fig. 6). In

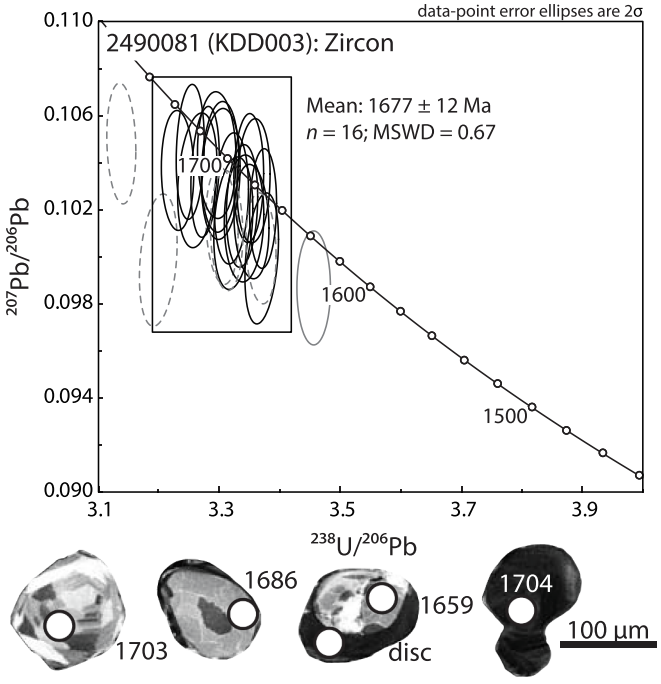

Fig. 6. Metamorphic zircon geochronology from sample 2490081, drill hole KDD003. All ages are $^{207}Pb/^{206}Pb$ ages. All data-point error ellipses on the concordia plots are 2σ, uncertainty on weighted average age is given to 95% confidence. Concordant analyses that are not included in the calculation of weighted mean ages are shown as grey ellipses; discordant analyses are shown as dashed ellipses.

CL images, most zircon grains display bright sector zoning, which may be overgrown by thin (~5–30 μm), dark rims. Rare grains are homogenous with low CL response. All zircon grains have morphologies typical of metamorphic zircon, flat HREE patterns and Th/U ratios between 0.04 and 1.01. Twenty-two analyses were collected from 18 grains. Five analyses are discordant and were excluded from further interpretation. A weighted mean $^{207}Pb/^{206}Pb$ age of the oldest 16 analyses is 1677 ± 12 (Fig. 6; MSWD = 0.67, prob. = 0.81). Within this population there is no relationship between age and trace element character, zoning patterns or CL response. The youngest concordant analysis has a distinctly younger $^{206}Pb/^{238}U$ age and elevated LREE contents compared to the main population, so was excluded.

Monazite grains in 2490081 are 100–250 μm in diameter and display complex, patchy zoning and variable BSE responses between grains. Forty-six analyses were collected from 11 grains mounted in epoxy resin. Eight analyses are discordant and were excluded from calculations. The remaining analyses define three populations (Fig. 4c). The oldest population comes from coarse-grained monazite with complex zoning. The $^{207}Pb/^{206}Pb$ weighted mean age of this population is 1694 ± 6 Ma (n = 31, MSWD = 0.92, prob. = 0.59). The middle population comes from dark rims that occur on some monazite grains. The five analyses making up this population have a $^{207}Pb/^{206}Pb$ weighted mean age of 1568 ± 16 Ma (MSWD = 0.81, probability = 0.52). The two youngest analyses have $^{207}Pb/^{206}Pb$ ages of c. 1515 Ma and come from a single dark grain ~ 100 μm in diameter. Trace element data from this sample shows that the c. 1568 Ma analyses generally have lower LREE and higher HREE + Y than the older population (Appendix 5). The c. 1515 Ma analyses have lower Si and significantly higher Y contents than all other analyses.

Forty-one analyses of anhedral biotite at the margins of garnet and cordierite in sample 2490081 give an isochron age of 1394 ± 44 Ma (MSWD = 0.77).

In summary, KDD003 does not preserve information about the age of the protolith but records granulite facies metamorphism at c. 1690 Ma. The formation of retrograde cordierite-bearing reaction microstructures at the expense of garnet may have occurred at c. 1570 Ma or c. 1515 Ma, as both these age populations show an increase in Y + HREE relative to the main population consistent with garnet breakdown (e.g. Kelly et al., 2006).

4.2.2. Sample MW8 (outcrop)

Sample MW8 contains biotite, K-feldspar, plagioclase, sillimanite, cordierite, spinel, corundum ilmenite and two generations of garnet. The first generation of garnet is coarse-grained and contains inclusions of biotite, quartz, and weakly oriented fibrolite (Fig. 3f). Lensoidal cordierite-spinel ± corundum symplectites are commonly surrounded by coronas of biotite and rarely inclusion-free second-generation garnet (Fig. 3f). The sample contains a weakly developed foliation defined by matrix biotite that is deflected around coarse-grained garnet and the lensoidal cordierite domains. This sample's distinctive petrographic character is identical to samples described by Jagodzinski et al. (2007) and Forbes et al. (2011) from the nearby Moonlight Hills region to the south (Fig. 2). Forbes et al. (2011) interpreted the cordierite-spinel symplectites to have replaced andalusite.

Monazite grains in MW8 are small (typically 20–40 μm in diameter) and unzoned in BSE images. Monazite grains are located throughout the matrix, as inclusions in garnet and biotite and rarely in the cordierite–spinel symplectites. Thirty-nine analyses were collected from 38 grains. Nine analyses were excluded on the basis of discordance and an additional two analyses were excluded because of high silica contents, suggesting contamination from the surrounding silicate mineral assemblage. The remaining analyses range in $^{207}Pb/^{206}Pb$ age from 1672 to 1534 Ma (Fig. 4c). Two groups can be differentiated on the basis of Y and Th/U ratios. In general, the high Y, high HREE analyses are older. Due to the small number of monazite grains in key microstructural locations and the relatively high number of discordant analyses, it is difficult to link monazite chemistry, age and microstructural location. Two grains located in the garnet coronas are part of the low Y monazite population, whereas of the two grains located within the first-generation garnet porphyroblasts, one was part of the high Y population and the other was discordant. A weighted mean age of each of these populations does not give a statistically valid age, however, this sample is interpreted to contain a Kimban-aged monazite population (c. 1670 Ma) that has been variably reset by metamorphism between c. 1580–1560 Ma. The older event is interpreted to have formed the garnet porphyroblasts and matrix assemblage, whereas the younger event is interpreted to have formed the cordierite-spinel domains and the second generation of garnet.

No Rb–Sr data were collected from this sample.

4.3. Samples adjacent to shear zones

4.3.1. Sample 2332807 and 2332809 (DDHARMN 1)

Sample 2332807 is a foliated gneiss containing biotite, garnet, sillimanite, magnetite and quartzofeldspathic leucosomes. The sample is heterogenous, containing varying abundances of feldspar, quartz and sillimanite on the scale of a thin section. It is interpreted to have a metasedimentary protolith. Sample 2332809 is located in the same drill hole and contains a similar mineralogy, but has a stronger gneissic fabric defined by abundant biotite and deformed magnetite.

Monazite grains in 2332807 are typically anhedral and located along grain boundaries in the foliated matrix. Fourteen analyses were collected in thin section from eight grains. One analysis was excluded on the basis of discordance. The remaining analyses define two groups (Fig. 4c). The first group has a $^{207}Pb/^{206}Pb$ weighed mean age of 1683 ± 13 Ma (n = 8, MSWD = 1.04, prob. = 0.40). The younger group give a $^{207}Pb/^{206}Pb$ weighed mean age of 1549 ± 18 Ma (n = 4, MSWD = 0.27, prob. = 0.85). The younger group has distinctly higher Eu and Yb contents than the older analyses (Appendix 5). A single concordant analysis with a $^{207}Pb/^{206}Pb$ age of 1627 ± 37 Ma is likely to be a mixed age. There is no obvious link between age and microstructural location.

Forty-six analyses of foliated biotite from sample 2332807 give an isochron age of 1453 ± 29 Ma (MSWD = 0.8), whereas 55 analyses from 2332809 give an isochron age of 1425 ± 27 Ma (MSWD = 0.94).

4.3.2. Sample 2449515 and 2499516 (TORCH 93RC 5)

Samples 2449515 and 2449516 are separated by less than two metres and come from an interval of strongly foliated schist containing muscovite, biotite, K-feldspar, quartz, magnetite, plagioclase and minor amounts of apatite. Sample 2449515 was used for monazite geochronology and sample 2499516 was used zircon geochronology. There are no significant textural or compositional differences between the two samples.

Zircon grains in 2449516 are 100–250 μm in length with aspect ratios of 1:2 and rounded to prismatic terminations. In CL images they are strongly luminescent, oscillatory zoned and rarely have small, dark metamict cores (Fig. 5d). Thirty-two analyses were collected from oscillatory zoned domains on 41 zircon grains. The majority of zircon grains in this sample have been affected by recent Pb loss, and many of them are discordant (Fig. 5d). Ten concordant analyses define a single age peak with a weighted mean $^{207}Pb/^{206}Pb$ age of 1755 ± 9 Ma (MSWD = 1.03, prob. = 0.42). The Th/U ratios of the concordant analyses range between 0.46 and 1.68 and show no trend with age. The remaining discordant analyses also have $^{207}Pb/^{206}Pb$ ages of c. 1750 Ma, with the exception of one grain, that has an older age of 2567 Ma (5% discordant). This sample does not record any significant metamorphic zircon growth.

Monazite grains are 100–250 μm in diameter, rounded and show patchy zoning in BSE images. Twenty-two analyses were collected from seven grains mounted in epoxy resin. One analysis was excluded on the basis of discordance. The remaining 21 analyses form a single population with a $^{207}Pb/^{206}Pb$ weighted mean age of 1567 ± 8 Ma (Fig. 4c; MSWD = 0.41; probability = 0.99).

Forty-four analyses of foliated biotite from sample 2449516 give an isochron age of 1442 ± 21 Ma (MSWD = 0.57).

In summary, drill hole TORCH 93RC 5 contains a metapelitic protolith that was deposited after c. 1750 Ma and was metamorphosed at c. 1567 Ma.

4.3.3. Sample 2345927 (SR 2)

Sample 2345927 is a strongly foliated metapelitic gneiss containing abundant sillimanite, biotite, garnet, cordierite, ilmenite and quartzofeldspathic leucosomes. Elongate cordierite moats contain inclusions of foliated sillimanite, biotite and ilmenite and rare garnet (Fig. 3g).

Monazite grains are 30–150 μm in diameter, equant to elongate and typically located within or adjacent to variably altered cordierite–sillimanite domains. Twenty-two analyses were collected in situ from 11 grains. One analysis was excluded on the basis of discordance. The remaining monazite yields a range of ages from 1613 to 1478 Ma and does not form a statistical single population (Fig. 4c). The majority of analyses yield ages of c. 1580 Ma, with a group of analyses at c. 1490 Ma. Support for the notion of two ages is given by the 'unmix' function within Isoplot 4.15 (Ludwig, 2012), which gives two ages of 1577 ± 10 Ma and 1501 ± 22 Ma, albeit with a high relative misfit of 0.85. There is no clear link between REE chemistry and age that could be used to better define these two populations, and grains that yield young analyses also yield older or mixed ages.

Fifty-four analyses of foliated biotite from sample 2345927 yield an isochron age of 1455 ± 30 Ma (MSWD = 0.63).

5. Results: *P–T* modelling

The geochronology suggests that the Mount Woods Domain records a polymetamorphic history. Phase equilibria modelling in polymetamorphic terranes can be challenging because there is the potential that the rocks record composite mineral assemblages (Morrissey et al., 2016a; Yakymchuk et al., 2015). Therefore, *P–T* pseudosections were calculated for two samples that record relatively simple monazite age populations and no petrological evidence for mineral reaction microstructures. This is done with the aim of providing constraints on the peak *P–T* conditions and thermal gradients of the c. 1700 Ma event. The *P–T* conditions of the younger events cannot be constrained because the only sample that gives a single Mesoproterozoic age (sample 2449515) does not contain a thermobarometrically sensitive mineral assemblage.

5.1. Sample 2490078 (WC05D001)

The peak assemblage in sample 2490078 is garnet, sillimanite, K-feldspar, cordierite, magnetite and quartz. Biotite is not abundant and predominantly occurs adjacent to garnet and domains of altered cordierite, where it forms anhedral, platy grains with no preferred orientation. Biotite also occurs rarely as a foliated mineral in the leucosome domains and in fractures within sillimanite and garnet. Biotite is therefore not interpreted to be part of the peak assemblage. Cordierite is very abundant, and in some parts of the sample cordierite separates coarse-grained garnet and sillimanite (Fig. 3c). However, in other parts of the sample coarse-grained sillimanite and garnet are not surrounded by cordierite, and therefore all three minerals are interpreted to form part of the peak assemblage. This sample contains magnetite and ilmenite so was calculated with a moderately oxidised bulk composition (Appendix 3). The peak assemblage occurs between 4.2 and 5.3 kbar and 800–840 °C (Fig. 7a). It is bounded to lower temperatures by the solidus and the absence of peak biotite, and to higher temperatures by the absence of spinel. Modelled modal abundances do not vary significantly across the peak field and do not further constrain conditions, but approximately correspond to the modal abundance of minerals observed in the rock.

5.2. Sample 2345929 (CD93 4)

The peak assemblage in sample 2345929 is interpreted to be garnet, plagioclase, K-feldspar, biotite, altered cordierite (now pinnite), quartz and silicate melt (Fig. 3d). This sample contains graphite but no Fe-oxides so the pseudosection was calculated using a reduced bulk composition (Appendix 3). The peak assemblage occurs between 4 and 6 kbar and 800–840 °C (Fig. 7b). The absence of sillimanite and orthopyroxene in the sample provide an upper and lower pressure constraint, respectively. The absence of ilmenite from the sample provides an upper temperature constraint that does not significantly vary with small differences in oxidation state (Appendix 3). The modal proportions of garnet, biotite and cordierite do not vary significantly across the peak field and so cannot be used to better constrain the *P–T* conditions.

6. Discussion

6.1. New protolith ages for the Mount Woods Domain

A range of new protolith ages are revealed in this study and are discussed from oldest to youngest. Detrital zircon geochronology from two metasedimentary samples from drill hole WC07D01 dominantly yields Archean ages of 2800–2550 Ma (Fig. 5a, b). Many of the zircon analyses in these samples display Pb loss and are moderately to highly discordant, making it difficult to unambiguously constrain the maximum depositional age. Similar detrital age peaks between 2800 and 2600 Ma are common in the Christie Gneiss of the adjacent Mulgathing Complex (Fig. 1), which was deposited after c. 2480 Ma but prior to ca. 2440 Ma (Reid et al., 2014b). It is likely that the metasedimentary rocks in drill hole WC07D01 are equivalent Neoarchean to earliest Palaeoproterozoic sedimentary rocks. Monazite geochronology from a garnet-bearing granite from drill hole Fire in the Sky gives an upper intercept age of 2471 ± 12 Ma (Fig. 4a), which may reflect the approximate magmatic age of the protolith. The new Archean to earliest Paleoproterozoic monazite and zircon ages from drill holes WC07D01 and

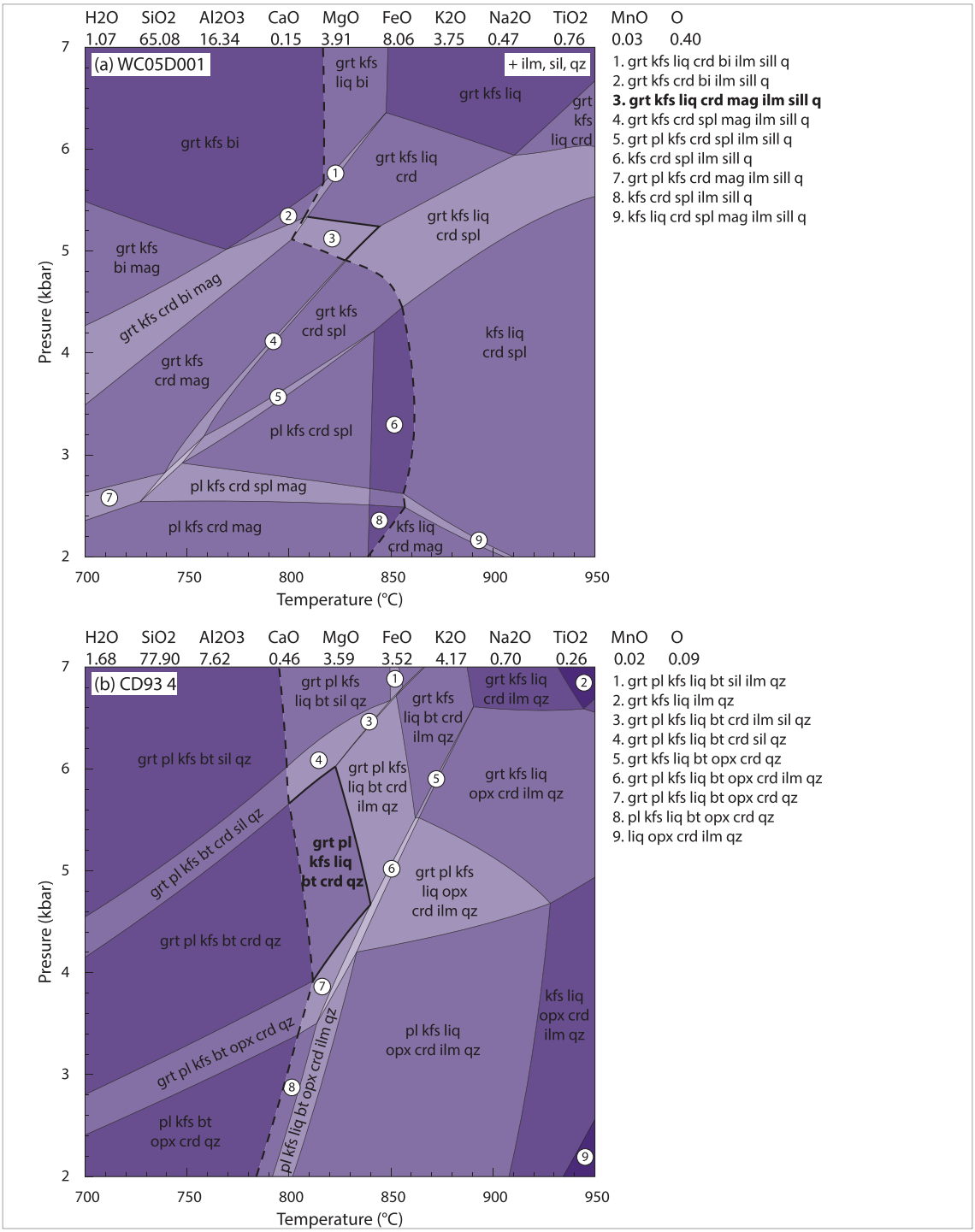

Fig. 7. Pressure–temperature (*P–T*) pseudosections for samples containing single c. 1700 Ma monazite populations. The peak field is outlined in bold and the dashed line is the solidus. The bulk composition in mol% is given above each pseudosection. (a) 2490078 (WC05D001). (b) 2345929 (CD93 4).

Fire in the Sky are the oldest known protolith ages from the Mount Woods Domain (Fig. 8a). Reconnaissance geochronology from a tonalite in the central part of Mount Woods yielded highly discordant early Paleoproterozoic zircon (Reid, 2013), and Archean rocks have previously been noted in the vicinity of Prominent Hill to the south of the Mount Woods Domain (Freeman and Tomkinson, 2010), which supports the presence of Archean basement in the region. The Archean to earliest Paleoproterozoic ages are similar to protolith ages of 2555–2440 Ma in the outcropping Sleaford and Mulgathing Complexes in the southern and central Gawler Craton, respectively (Fig. 1; Brown et al., 2022; Reid et al., 2014b; Swain et al., 2005), and suggest that the Mount Woods region is underlain by Sleaford and Mulgathing Complex equivalents. This supports the notion that much of the Paleo- to Mesoproterozoic crust of the Gawler Craton is underlain by Archean basement.

Previous work has identified the presence of three sedimentary sequences in the Mount Woods region, although these have been defined from relatively few samples (Fig. 8a). A single sample of the Mount Woods Metamorphics in the westernmost part of the central zone contains a single detrital zircon peak at c. 1860 Ma (Tiddy et al., 2020). The Skylark Metasediments are characterised by a unimodal c. 1750 Ma

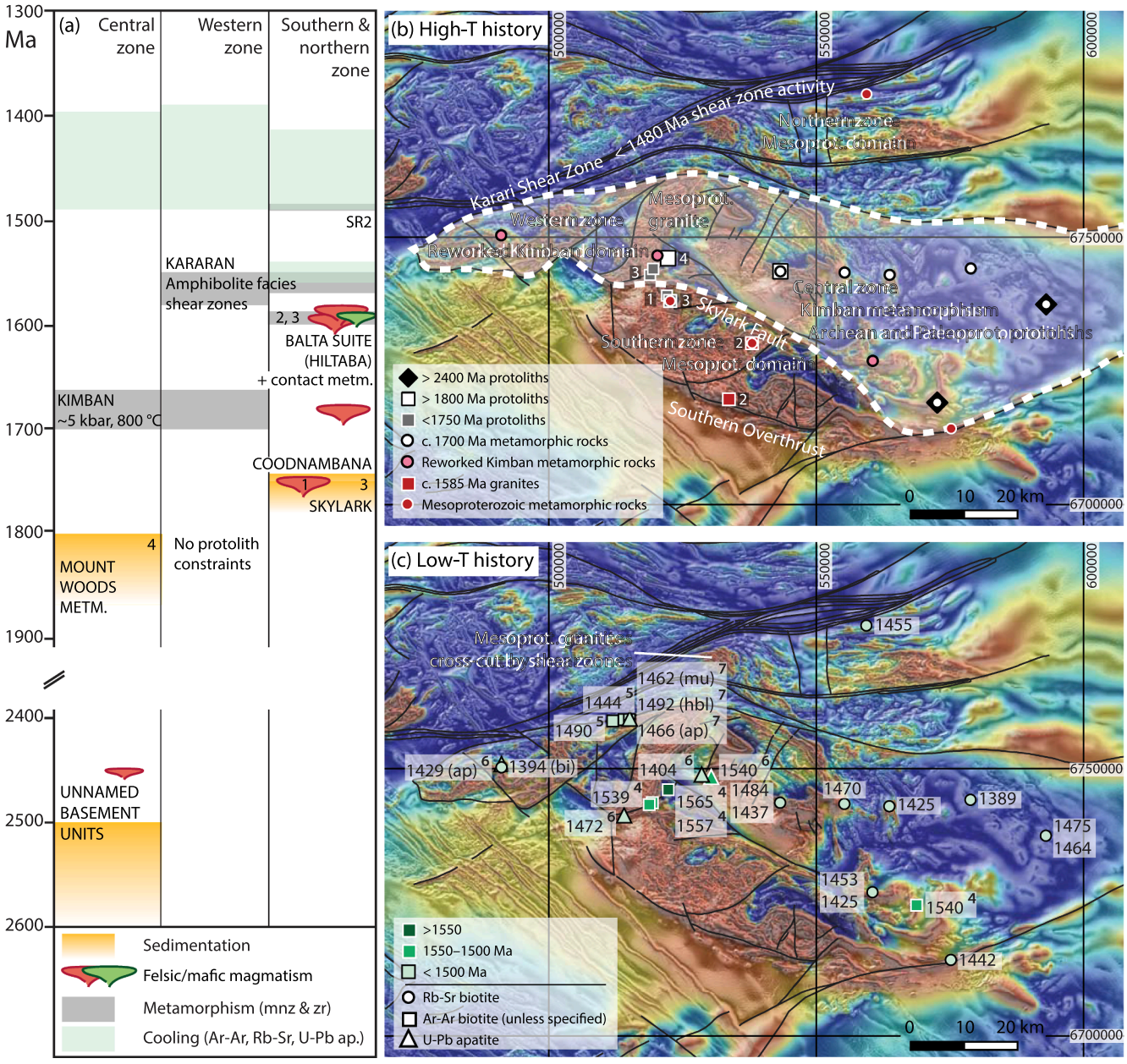

Fig. 8. Summary of geochronology from the Mount Woods region. Ages are from this study, with additional geochronology from (1) Fanning et al., 1988; (2) Jagodzinski, 2005; (3) Jagodzinski et al., 2007; (4) Tiddy et al., 2020, which also includes updated Ar–Ar ages from Forbes et al., 2012; (5) Fraser et al., 2012; (6) Hall et al., 2018; (7) Jagodzinski and Reid, 2017. (a) Time–space plot for the three zones of the Mount Woods Domain. (b) Spatial distribution of protolith ages and high temperature metamorphic geochronology from U–Pb zircon and monazite. (c) Spatial distribution of low temperature thermochronology from Rb–Sr biotite, Ar–Ar mica and hornblende and U–Pb apatite.

detrital zircon age peak, and are interpreted to be a volcaniclastic sequence deposited after c. 1750 Ma (Jagodzinski et al., 2007; Tiddy et al., 2020). The Coodnambana Metaconglomerate unconformably overlies the Skylark Metasediments and contains a dominant c. 1750 Ma detrital zircon peak with a very minor c. 1850 Ma component, thought to be derived from the Skylark Metasediments (Jagodzinski et al., 2007).

A sample of garnet-bearing gneiss from drill hole CD93 4 contains concordant analyses that range in age between 1925 and 1755 Ma and define an apparent age peak at c. 1860 Ma, suggesting it is equivalent to the Mount Woods Metamorphics. This sample has experienced Pb loss, meaning that care must be taken when interpreting maximum depositional ages from single analyses (Herriott et al., 2019). A conservative maximum depositional age for this sequence of 1855 ± 5 Ma is given by 70 concordant analyses (Fig. 5c), with a minimum depositional age given by the c. 1690 Ma metamorphic monazite age for this sample (Fig. 4b). A proximal source of the c. 1850–1860 Ma detrital zircon may be the c. 1850 Ma Donington Suite, which underlies the c. 1750 Ma Wallaroo Group in the Olympic Domain to the south (Fig. 1; Jagodzinski, 2005; Reid et al., 2008). Detrital zircon ages of 1880–1800 Ma are also common in metasedimentary rocks and meta-volcaniclastics of the Lander Rock Formation in the Aileron Province in the North Australian Craton (Claoué-Long et al., 2008), suggesting that the Mount Woods Metamorphics may be correlatives of these units and/or received detritus from northern Australia. Metasedimentary rocks with maximum depositional ages of c. 1840 Ma from the Peake and Denison Domain (Fig. 1) have also been suggested to have similar providence to the Lander Rock Formation, which may support this interpretation (Reid et al., 2017).

A sample of K-feldspar–biotite–muscovite schist from drill hole TORCH 93RC 5 contains concordant analyses that range in age from 1783 to 1727 Ma and define an age peak at c. 1750 Ma, with one near-concordant older grain at c. 2500 Ma. This sample does not record any significant metamorphic zircon growth but does contain metamorphic monazite with a weighted mean age of 1567 ± 8 Ma (Fig. 4c, section 6.2). The depositional interval and detrital zircon spectra suggest that the metasedimentary sample from drill hole TORCH 93RC 5 is equivalent to the Skylark Metasediments. The precise source of the c. 1750 Ma detrital zircon is uncertain. Magmatic rocks with ages of c. 1750 Ma are not known from the Mount Woods Domain, but 1775–1750 Ma orthogneiss occurs in the northern Gawler Craton (Howard et al., 2011b) and c. 1790–1740 Ma zircon is common in volcaniclastic sediments in the Gawler Craton (e.g. Reid and Hand, 2012).

Although there are limited data available, the Mount Woods region appears to contain at least four metasedimentary sequences (Fig. 8a, b). Archean to earliest Paleoproterozoic metasedimentary rocks and the post-c. 1855 Ma Mount Woods Metamorphics occur in the central zone. The Skylark Metasediments and Coodnambana Metaconglomerate were deposited after c. 1750 Ma and are exposed in the southern zone.

6.2. *New constraints on timing and P–T conditions of metamorphism in the Mount Woods Domain*

Detrital monazite is uncommon in amphibolite to granulite facies metasedimentary rocks because it is thought to be highly reactive in the presence of fluids and melts generated during prograde metamorphism (e.g. Kohn and Malloy, 2004; Williams et al., 2011; Yakymchuk, 2017). We therefore interpret the monazite ages from our metasedimentary rocks to be metamorphic. The new monazite U–Pb data shows that the Mount Woods Domain experienced at least three tectonothermal events. Prior to this study there was very little published metamorphic geochronology from the Mount Woods Domain. Therefore, the metamorphic record throughout much of the Mount Woods Domain was inferred rather than demonstrated (e.g. Tiddy et al., 2020).

6.2.1. *Kimban-aged metamorphism*

All samples from north of the Skylark Fault contain monazite age populations between c. 1700–1675 Ma (Fig. 8b), broadly corresponding to the age of the c. 1730–1690 Ma Kimban Orogeny elsewhere in the Gawler Craton (Reid and Hand, 2012). Sample 2345928 contains zoned monazite that yield two age populations, outside uncertainty of each other, at 1692 ± 5 Ma and 1675 ± 5 Ma (Fig. 4b). The significance of this is unclear, as the sample does not contain mineral reaction microstructures. Metamorphic zircon from drill hole KDD003, located in the westernmost part of the Mount Woods Domain, gives a $^{207}Pb/^{206}Pb$ weighted average age of 1677 ± 12 Ma (Fig. 6), which is slightly younger than the 1695 ± 5 Ma age for monazite in the sample (Fig. 4c). Therefore, granulite facies metamorphism in samples north of the Skylark Fault (comprising Archean–earliest Paleoproterozoic protoliths and the c. 1810 Ma Mount Woods Metamorphics) is interpreted to have occurred at c. 1700–1675 Ma.

Two samples from drill holes CD93 4 and WC05D001 in the central Mount Woods Domain were selected for phase equilibria modelling to constrain the conditions of Kimban-aged metamorphism (Fig. 7a, b). The phase equilibria models suggest peak conditions were 4.8–5.3 kbar and 800–840 °C, corresponding to apparent thermal gradients of 140–160 °C/kbar. The modelled solidus in these rocks occurs at temperatures of ~ 790–850 °C, reflecting that the rocks have lost melt.

6.2.2. *Early Mesoproterozoic metamorphism*

Existing zircon geochronology suggests that the rocks south of the Skylark Fault have protolith ages younger than c. 1750 Ma and metamorphic ages in the 1595–1575 Ma interval (Jagodzinski, 2005; Jagodzinski et al., 2007). These ages are coeval with the c. 1600–1570 Ma Hiltaba magmatic event, expressed in the Mount Woods region by granitic and gabbroic rocks with crystallisation ages between c. 1594–1584 Ma (Jagodzinski, 2005). Older CHIME monazite ages of c. 1615 ± 22 Ma and 1617 ± 18 Ma from the Moonlight Hills (Fig. 2) were interpreted to be prograde (Forbes et al., 2011).

The majority of Mesoproterozoic monazite ages in this study are younger than the c. 1594–1584 Ma magmatic rocks in the region and previously published metamorphic zircon ages (Jagodzinski, 2005; Jagodzinski et al., 2007). A possible exception is a sample of strongly sheared gneiss from drill hole SR2 in the northernmost Mount Woods Domain. This sample yields a range of monazite $^{207}Pb/^{206}Pb$ ages between 1601 and 1478 Ma, with a cluster of ages at c. 1580 Ma (Fig. 4c). This is interpreted to reflect resetting of a c. 1580 Ma monazite age population by deformation and/or metamorphism at c. 1480 Ma. Outcrop sample MW8 was selected for monazite geochronology due to its distinctive similarities to the sample analysed by Forbes et al. (2011) that yielded a c. 1615 Ma CHIME monazite age. However, although a pooled age of all concordant analyses from MW8 is c. 1620 Ma (MSWD = 10.3), the monazite chemistry and large MSWD indicates this is a mixed age (Appendix 5). The previously reported CHIME analyses are likely to have formed a single, statistically-valid population due to the large uncertainties on individual analyses from the CHIME method. The polymetamorphic nature of this sample is evident from the clear mineral reaction microstructures, where early garnet is overprinted by a matrix assemblage containing cordierite, biotite, spinel and a second generation of garnet (Fig. 3f). The timing of formation of the cordierite–spinel reaction textures is not well constrained and may have formed coeval with Hiltaba magmatism at c. 1590 Ma, but are more likely to have formed at c. 1570–1550 Ma, similar to the interpreted timing of shear zone activity in the region (below). The *P–T* conditions determined by Forbes et al. (2011) were constrained by superimposing *P–T* models for the cordierite–spinel domains and the matrix domain. However, this approach is invalid in polymetamorphic rocks. In addition, the formation of the cordierite–spinel symplectites may post-date the Hiltaba magmatism, meaning that this sample cannot unambiguously provide constraints on the *P–T* conditions at the time of Hiltaba magmatism in this region.

Drill hole TORCH 93RC 5 is located along a major ENE-trending shear zone in the southern Mount Woods Domain and gives a single monazite population of 1567 ± 8 Ma (Fig. 4c). Adjacent to the Skylark Fault, drill hole DDHARMN 1 gives a bimodal monazite population, with an older age of 1685 ± 14 Ma and a younger age of 1549 ± 15 Ma, which is just within uncertainty of the monazite age from the TORCH 93RC 5 drillhole. In the westernmost Mount Woods Domain, drill hole KDD003 contains three monazite age populations, including a small population at 1568 ± 16 Ma. The lack of c. 1590–1580 Ma ages in these samples suggests that shear zones in the Mount Woods Domain were not active during the Hiltaba magmatic event, but were instead active at c. 1570–1550 Ma. This corresponds to the accepted timing of structural reworking elsewhere in the Gawler Craton during the Kararan Orogeny (e.g. Daly et al., 1998; Payne et al., 2008). It is not possible to calculate tightly constrained *P–T* conditions for this event because the sample that contains only c. 1570 Ma monazite (TORCH 93RC 5) does not contain a mineral assemblage that is sensitive to changes in pressure and temperature. However, the presence of muscovite and K-feldspar and lack of evidence for partial melting suggest that it formed at upper amphibolite facies conditions.

6.2.3. *Post-1500 Ma metamorphism, shear zone reactivation and cooling*

Drill hole SR2 in the northernmost Mount Woods Domain sits in the extension of the Karari Shear Zone, and the younger c. 1500–1480 Ma monazite in this sample suggests the Karari Shear Zone was active at this time. This is broadly consistent with biotite $^{40}Ar–^{39}Ar$ ages of c. 1450 Ma from further west within the shear zone (Fraser et al., 2012). Biotite Ar–Ar ages from elsewhere in the Mount Woods region range between c. 1560 and 1444 Ma (Forbes et al., 2012; Fraser et al., 2012; Tiddy et al., 2020), whereas apatite U–Pb ages range from 1540 to 1404 Ma (Hall

et al., 2018). These ages come from a relatively small number of samples that are widely distributed, meaning it is difficult to interpret the significance of the range in ages.

The development of in situ Rb–Sr dating of biotite provides a method of collecting large amounts of data relatively quickly (Hogmalm et al., 2017; Zack and Hogmalm, 2016), allowing a number of samples from different parts of the Mount Woods region to be directly compared. All samples from the Mount Woods region give Rb–Sr biotite ages of c. 1480–1390, with the majority of ages around c. 1450 Ma (Fig. 8c). The closure temperature of the Rb–Sr system in biotite is likely to depend on factors such as grain size, modal proportion and chemical composition of biotite (Jenkin et al., 2001), but is assumed to be at least 300–400 °C (Del Moro et al., 1982). This suggests that the Mount Woods Domain cooled through mid-crustal temperatures at c. 1450 Ma. The significance of older Ar–Ar ages of c. 1540 Ma and c. 1560 Ma in the Mount Woods Domain (Forbes et al., 2012; Tiddy et al., 2020) is unclear in the light of the dominance of c. 1450 Ma Ar–Ar from elsewhere in Mount Woods (Fig. 8; Fraser et al., 2012; Jagodzinski and Reid, 2017) and the northern Gawler Craton (Reid and Forster, 2021). If the range of thermochronology ages is geologically meaningful, it may suggest slow or intermittent regional exhumation. The high thermal gradients in the Mount Woods Domain mean that down-thrown areas may remain hot, whereas small amounts of uplift on faults could allow other areas to cool below the closure temperature earlier. However, another alternative is that the metamorphic biotite previously dated by Ar–Ar contains 'cryptic' excess ^{40}Ar. Excess ^{40}Ar may be homogenously distributed throughout the crystal lattice, resulting in too old, yet apparently statistically valid, plateau ages that can only be identified through the use of other geochronometers (Scibiorski et al., 2021). Obtaining Rb–Sr ages from samples yielding old Ar–Ar ages, or biotite Ar–Ar ages from samples with in situ Rb–Sr ages, may help to determine the significance of the difference in age between the two systems.

6.3. Implications of the new data for tectonic models of the Mount Woods Domain

A variety of models for the tectonic history of the Mount Woods Domain have been proposed (e.g. Betts et al., 2003; Forbes et al., 2011; Tiddy et al., 2020). However, all of the previous tectonic models have been based on limited geochronology and inferred cross-cutting relationships in small numbers of field outcrops and in geophysical imagery. Most recently, Tiddy et al. (2020) argued for a metamorphic core complex in the Mount Woods region that developed at c. 1600–1580 Ma and was modified at c. 1570–1540 Ma. This is not supported by our geochronology, which suggests that the metamorphic mineral assemblages and structural fabrics observed in outcrop and geophysical imagery in the central Mount Woods zone are likely to record multiple stages of deformation during the Paleoproterozoic Kimban Orogeny (Fig. 8, Betts et al., 2003), rather than c. 1600–1580 Ma as would be expected in the core complex model. The rocks analysed from the major shear zones in this study yield monazite ages of c. 1570–1550 Ma, postdating the emplacement of Hiltaba magmas, and are consistent with the Kararan Orogeny. The lack of c. 1590–1580 Ma metamorphic ages in this study suggests that the Hiltaba Event may have caused localised contact metamorphism, rather than significant regional metamorphism and deformation.

6.4. Mount Woods as a piercing point for southern Proterozoic Australia

The multiple phases of deformation and metamorphism create the potential for composite fabrics and mineral assemblages, limiting the possible tectonic interpretations for individual events within the Mount Woods Domain. However, because the Mount Woods region contains a protolith and metamorphic history spanning c. 2500–1450 Ma, it is invaluable for drawing links between different parts of Proterozoic Australia. The protolith ages and recurring metamorphism identified in the Mount Woods Domain in this study correspond to phases of sedimentation and major tectonic events in the broader Gawler Craton, North Australian Craton (NAC), Curnamona Province and parts of Antarctica (Fig. 9).

Cawood and Korsch (2008) and Payne et al. (2009) propose that the NAC and SAC/Mawson Continent evolved as a coherent entity from the late Archean, termed the Diamantina Craton. In this model, a long-lived subduction zone to the southwest, and potentially also the northeast, of the continent drove repeated phases of back-arc extension and compression. In contrast, Betts et al. (2016) propose that Proterozoic Australia formed by via the accretion of a series of microcontinental ribbons onto the Archean core of the NAC by around c. 1800 Ma. After c. 1800 Ma, the southern margin of Australia is interpreted to be a long-lived convergent accretionary orogen with north-dipping subduction, dominated by extensional tectonics and slab rollback. In this model, the Mount Woods Domain, and more broadly the Nawa Domain of the northern Gawler Craton, sits on a microcontinental ribbon that extends into the southern NAC and is separate to the Archean core of the Gawler Craton and the c. 1850 Ma Donington Suite. Slab rollback is interpreted to result in detachment of the Archean ribbon of the Gawler Craton between 1800 and 1750 Ma, which was then reattached during the Kimban Orogeny (Betts et al., 2016). In contrast, our results indicate that the Mount Woods Domain is built on Archean to earliest Paleoproterozoic basement, equivalent to the Sleaford and Mulgathing Complexes in the Gawler Craton. The c. 1855 Ma Mount Woods Metamorphics contain detrital zircon spectra similar to those in the Lander Rock Formation in the Aileron Province (Claoué-Long et al., 2008) whereas detrital zircon in the Skylark Metasediments corresponds to the ages of magmatism in the northern Gawler Craton and Aileron Province (Howard et al., 2011b; Scrimgeour, 2013). Therefore, these new data highlight a long-term connection and shared evolution between the Mount Woods Domain, northern Gawler Craton/Aileron, and the Archean "core" of the Gawler Craton in the Paleoproterozoic (Fig. 9), and are not consistent with models suggesting a separate evolution.

By the mid-Paleoproterozoic, most tectonic models agree that the NAC and Mawson Continent were contiguous and share a similar metamorphic history from c. 1730 Ma (Fig. 9). The overall tectonic setting of Australia in the Proterozoic is difficult to interrogate because key regions are relatively poorly exposed and many of the significant structures record multiple phases of reactivation, meaning it is difficult to determine a sense of displacement or kinematics. However, proxies such as the thermal character of metamorphism and its timing relative to ages of magmatism and sedimentation can be used to assess the relationships between major crustal blocks (Fig. 9). The c. 1730–1690 Ma Kimban Orogeny is the most pervasive tectonometamorphic event in the Gawler Craton. It is expressed as mid-*P* transpressional deformation within the Kalinjala Shear Zone in the southern Gawler Craton (Fig. 1; Dutch et al., 2010; Vassallo and Wilson, 2002). Elsewhere in the Gawler Craton it is expressed as dominantly high thermal gradient metamorphism (this study; Morrissey et al., 2016b; Reid et al., 2019; Williams et al., 2018) and widespread mafic to felsic magmatism (Wade and McAvaney, 2017). The Kimban Orogeny extends into the NAC and East Antarctica as the Strangways and Nimrod Orogenies, respectively (Fig. 9; Goodge and Fanning, 2016; Scrimgeour, 2013). The Kimban–Strangways–Nimrod Orogeny was previously proposed to reflect continental collision along the margin of the Mawson Continent at c. 1730 Ma (e.g. Betts et al., 2008; Boger, 2011; Payne et al., 2009). This was primarily based on the interpretation that eclogite facies metamorphism in the Miller Range in Antarctica during the Nimrod Orogeny could be linked to mid-*P* metamorphism in the Kalinjala Shear Zone in the southern Gawler Craton (Betts et al., 2008; Goodge and Fanning, 2016; Payne et al., 2009). However, recent zircon petrochronology from the Miller Range demonstrates that the high-*P* metamorphism is actually Cambrian in age, with Paleoproterozoic zircon likely to be mafic igneous in origin (Brown et al., 2021). Therefore, the c. 1730–1690 Ma interval in Antarctica, the Gawler Craton and northern Australia is

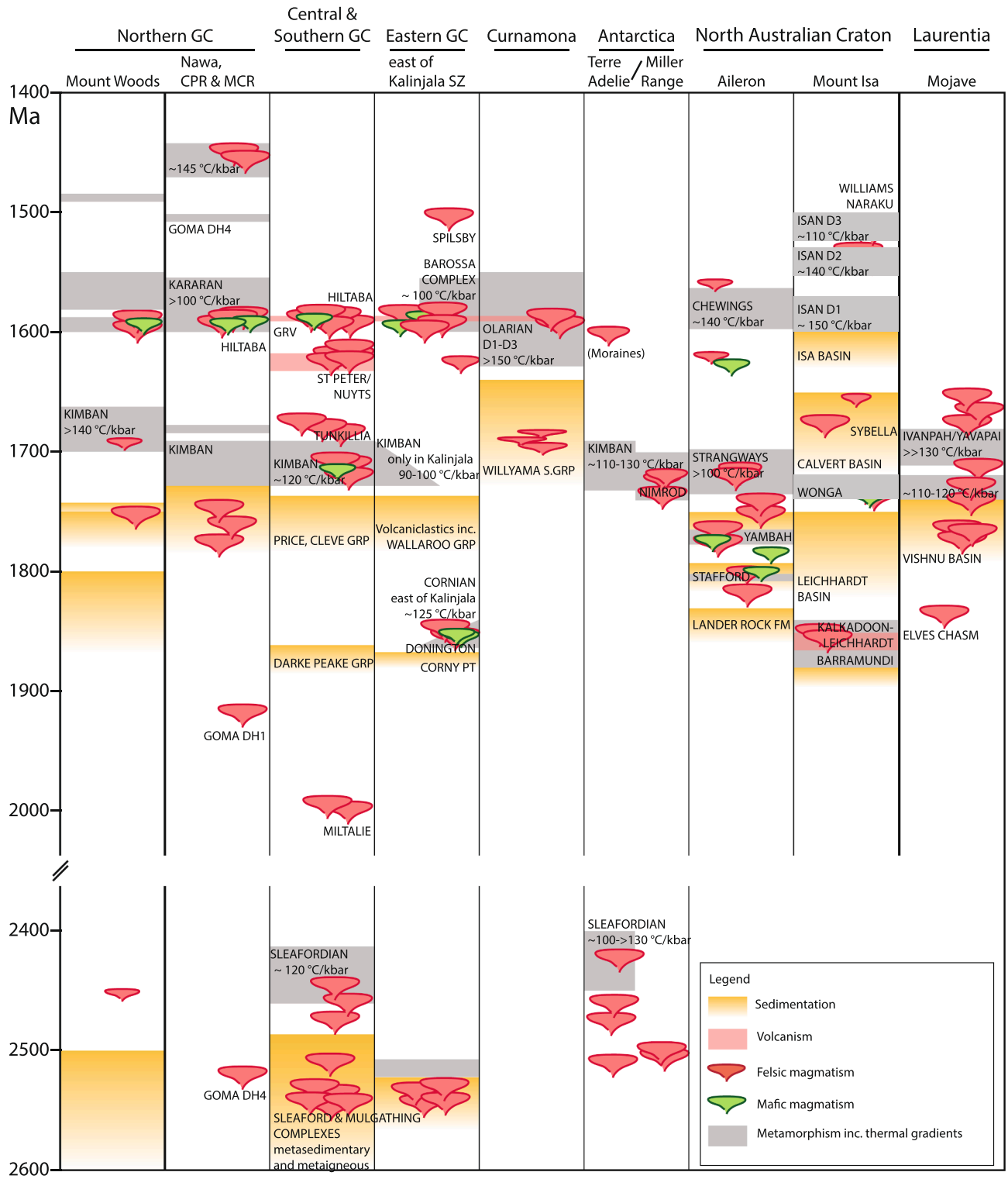

Fig. 9. Time–space plot showing the Mount Woods Domain in a broader context with key timelines from selected regions in the SAC, NAC, east Antarctica and the Mojave Province in western Laurentia. Time-space plot for the northern Gawler Craton adapted from Reid and Forster (2021); southern and eastern Gawler Craton from Reid and Hand (2012); Curnamona Province from De Vries Van Leeuwen et al. (2022); Terre Adelie from Williams et al., (2018) with additional data from Peucat et al. (2002); Miller Range/Nimrod Complex from Goodge and Fanning (2016); Aileron Province from Scrimgeour (2013); Mount Isa from Olierook et al. (2022); and the Mojave Province from Holland et al. (2018).

predominantly associated with high thermal gradient metamorphism and magmatism (Brown et al., 2021). Prior to c. 1730 Ma, the NAC and SAC were dominated by widespread basin development and punctuated intrusive and extrusive magmatism (Fanning et al., 2007; Hand et al., 2007; Howard et al., 2011a; Lane et al., 2015; Payne et al., 2006; Reid and Hand, 2012; Scrimgeour, 2013; Szpunar et al., 2011). The elevated thermal gradients during c. 1730–1690 Ma metamorphism is consistent with a tectonic setting involving high heat flow and thinned crust that may have been inherited from an extensional setting prior to metamorphism.

In the late Paleoproterozoic to early Mesoproterozoic, southern and eastern Australia experienced a rapid succession of magmatic and metamorphic events. The locus and timing of these events varies across the continent, but all are characterised by high to very high thermal gradients, variable amounts of magmatism and are broadly associated with shortening (Fig. 9). In the Mount Isa and Georgetown Inliers in the NAC, the c. 1600 Ma event is proposed to reflect collision of Australia with Laurentia (e.g. Pourteau et al., 2018; Volante et al., 2020) followed by extension-driven magmatism between 1560 and 1490 Ma (Volante et al., 2022). At this time the Gawler Craton records the c. 1595–1570 Ma Hiltaba–GRV large igneous province (Jagodzinski et al., 2023), followed by deformation during the Kararan Orogeny at c. 1570–1540 Ma (Hand et al., 2007). After c. 1500 Ma, the NAC and SAC are thought to have progressively separated into the distinct cratonic blocks separated by mid-Mesoproterozoic orogenic belts (Fig. 1b). The 1490–1450 Ma timeline involves the development of intractratonic basins (Beyer et al., 2018; Cherry et al., 2017) and regional resetting of low temperature geochronometers in the NAC and SAC (Fraser et al., 2012; Fraser and Lyons, 2006; Reid and Forster, 2021). High thermal gradient, granulite facies metamorphism and A-type magmatism also occurs at c. 1450 Ma in the northern Gawler Craton (Morrissey et al., 2019). The high thermal gradients, A-type magmatism, rift basin development and regional isotope resetting in eastern Proterozoic Australia are interpreted to be evidence for extension, potentially related to rifting of the SAC from the NAC, or rifting between Australia and Laurentia during Nuna breakup (Morrissey et al., 2019).

The high thermal gradient metamorphism, intermittent magmatism and protracted sedimentary record throughout the NAC and SAC is consistent with an overall extensional regime that spans the majority of the Paleoproterozoic (Fig. 9). This process created thin crust and extensional basins that were periodically inverted by transient shortening, but without creating significant crustal thickening and without leading to complete detachment or removal of crustal ribbons (e.g. Collins, 2002a; Collins, 2002b; Giles et al., 2002). Rifting and the attainment of high temperatures during metamorphism may have been facilitated by long-term crustal weakening caused by the abundance of high heat producing rocks in Proterozoic Australia (McLaren et al., 2003). The direction of rifting and extension was likely to have varied, controlled by varying stresses transmitted from convergent margins along the southern margin of the combined NAC/SAC in the late Paleoproterozoic, and to the northeast associated with the amalgamation, and then separation, of Australia and Laurentia in the late Paleoproterozoic to early Mesoproterozoic (e.g. Aitken et al., 2016; Morrissey et al., 2019; Pourteau et al., 2018; Volante et al., 2020).

6.5. *Proterozoic Australia in Nuna: Links with western Laurentia*

The Mount Woods Domain is an important tie point in supercontinent reconstructions with western Laurentia, because it is the most easterly known point on the Gawler Craton that preserves direct evidence of the Archean basement as well as Paleo- to Mesoproterozoic tectonism. Although a connection between Australia and Laurentia in the Mesoproterozoic is well accepted, a connection between Australia and Laurentia in the Paleoproterozoic is debated (e.g. Betts et al., 2008; Holland et al., 2018; Kirscher et al., 2020; Payne et al., 2009; Pourteau et al., 2018). Paleoproterozoic sediments in eastern Australia deposited after c. 1650 Ma record juvenile input that is not consistent with known Australian source regions, and is proposed to be derived from Laurentia (Barovich and Hand, 2008). However, most Laurentian Paleoproterozoic sedimentary rocks appear to be derived from Laurentian sources, and therefore do not require a connection between Australia and Laurentia in the Paleoproterozoic (Brennan et al., 2021). An exception to this is the ~1790–1750 Ma Vishnu Basin in the Mojave Province in southwestern Laurentia. The Vishnu Basin contains detrital zircon populations at c. 1850–2100 Ma and 2400–2900 Ma that are isotopically similar to coeval rocks in the Mawson Continent (Holland et al., 2018). More broadly, the Mojave Province also contains c. 1840 Ma tonalite gneiss and 1790–1730 Ma calc-alkaline magmatism. High thermal gradient metamorphism between c. 1710–1680 Ma was followed by c. 1690–1650 Ma potassic magmatism (Holland et al., 2018). The detrital zircon populations, timing of sedimentation and magmatism and thermal character of metamorphism are similar to that seen in the Mount Woods Domain and surrounding rocks of the Gawler Craton (Fig. 9). This supports a Mojave–Australia connection at c. 1800 Ma, with the potential that the Mojave Province was located proximal to the Gawler Craton. Alternatively, Gibson and Champion (2019) suggest that the Mojave province may in fact be a piece of Australian crust that has been stranded in Laurentia after Mesoproterozoic rifting. In this model, there is no requirement for a connection between Australia and Laurentia in the Paleoproterozoic. Instead, given the Mojave Province experienced calc-alkaline magmatism from 1790 to 1730 Ma while the Gawler Craton was undergoing extensive basin formation, it is conceivable that the Mojave Province represents the active margin of the Mawson Continent. The pre-Kimban extension of the Gawler Craton/Mawson Continent then represents a back-arc or distal basin to this active margin.

7. Conclusions

Basement-intersecting drill holes in the Mount Woods Domain reveal a protracted history of sedimentation, magmatism, metamorphism, deformation, and cooling between 2500 and 1450 Ma. The central Mount Woods Domain comprises Archean to earliest Paleoproterozoic metasedimentary rocks and garnet-bearing granite with protolith ages of c. 2500–2400 Ma and metasedimentary rocks deposited after c. 1855 Ma. These were metamorphosed under high thermal gradients to *P–T* conditions of 4.8–5.3 kbar and 800–840 °C during the Kimban Orogeny, c. 1700–1670 Ma. The southern Mount Woods Domain contains metasedimentary rocks deposited after c. 1750 Ma that have been metamorphosed to amphibolite facies and intruded by c. 1590 Ma granite and gabbro. Major shear zones such as the Skylark Fault were active between c. 1570–1550 Ma, with another phase of shear zone activity at c. 1480 Ma in the northern Mount Woods Domain. The preservation of Kimban-aged structures and metamorphic mineral assemblages in the central Mount Woods Domain may suggest that it is a low-strain zone that is wrapped by Mesoproterozoic high strain zones active between c. 1570–1480 Ma. Shear zone activity at c. 1480 Ma may have facilitated exhumation and cooling of the Mount Woods region, with Rb–Sr biotite ages throughout the Mount Woods Domain giving ages between c. 1480–1390 Ma. The tectonic record in the Mount Woods Domain corresponds to events seen more broadly in the Gawler Craton and North Australian Craton, and contributes to the recognition of a long-lived connection between the SAC and NAC in the Proterozoic.

CRediT authorship contribution statement

Laura J. Morrissey: Writing – review & editing, Conceptualization. **Justin L. Payne:** Writing – review & editing, Conceptualization. **Martin Hand:** Writing – review & editing. **Chris Clark:** Writing – review & editing. **Matthew Janicki:** .

Declaration of Competing Interest

The authors declare that they have no known competing financial interests or personal relationships that could have appeared to influence the work reported in this paper.

Data availability

Data is available in the supplementary files

Acknowledgements

S Gilbert, B Wade and A McFadden are thanked for technical support at Adelaide Microscopy. This project was supported by ARC Linkage Project LP160100578 (JP and MH) and the Mineral Exploration Cooperative Research Centre (MinEX CRC). This is MinEX CRC document number 2023/6. LJM is supported by an ARC DECRA Fellowship DE210101126 and funding from UniSA.

Appendix A. Supplementary data

Supplementary data to this article can be found online at https://doi.org/10.1016/j.precamres.2023.107077.

References

Aitken, A.R.A., Betts, P.G., Young, D.A., Blankenship, D.D., Roberts, J.L., Siegert, M.J., 2016. The Australo-Antarctic Columbia to Gondwana transition. Gondwana Research 29, 136–152.

Allen, M., Anderson, I., Benavides, J., Betts, P., Bull, S., Creaser, R., Davidson, G., Freeman, H., Holcombe, R., Murphy, F., 2016. New geological and geochronological constraints on the origin of the Prominent Hill hematitic IOCG deposit, Gawler craton, South Australia, Australian Earth Science Convention, Uncover Earth's Past to Discover our Future, Adelaide, Australia, Adelaide, p. 1.

Armit, R., Betts, P.G., Schaefer, B.F., Yi, K., Kim, Y., Dutch, R.A., Reid, A., Jagodzinski, L., Giles, D., Ailleres, L., 2017. Late Palaeoproterozoic evolution of the buried northern Gawler Craton. Precambrian Research 291, 178–201.

Barovich, K., Hand, M., 2008. Tectonic setting and provenance of the Paleoproterozoic Willyama Supergroup, Curnamona Province, Australia: Geochemical and Nd isotopic constraints on contrasting source terrain components. Precambrian Research 166, 318–337.

Belousova, E.A., Reid, A.J., Griffin, W.L., O'Reilly, S.Y., 2009. Rejuvenation vs. recycling of Archean crust in the Gawler Craton, South Australia: Evidence from U-Pb and Hf isotopes in detrital zircon. Lithos 113, 570–582.

Betts, P.G., Armit, R.J., Stewart, J., Aitken, A.R.A., Ailleres, L., Donchak, P., Hutton, L., Withnall, I., Giles, D., 2016. Australia and Nuna, in: Li, Z.X., Evans, D.A.D., Murphy, J.B. (Eds.), Supercontinent Cycles Through Earth History. Geological Society, London, Special Publications, pp. 47-81.

Betts, P.G., Valenta, R.K., Finlay, J., 2003. Evolution of the Mount Woods Inlier, northern Gawler Craton, Southern Australia: an integrated structural and aeromagnetic analysis. Tectonophysics 366, 83–111.

Betts, P.G., Giles, D., Schaefer, B.F., 2008. Comparing 1800–1600 Ma accretionary and basin processes in Australia and Laurentia: Possible geographic connections in Columbia. Precambrian Research 166, 81–92.

Beyer, S.R., Kyser, K., Polito, P.A., Fraser, G.L., 2018. Mesoproterozoic rift sedimentation, fluid events and uranium prospectivity in the Cariewerloo Basin, Gawler Craton, South Australia. Australian Journal of Earth Sciences 65, 409–426.

Boger, S.D., 2011. Antarctica — Before and after Gondwana. Gondwana Research 19, 335–371.

Brennan, D.T., Brian Mahoney, J., Li, Z.-X., Link, P.K., Evans, N.J., Johnson, T.E., 2021. Detrital zircon U-Pb and Hf signatures of Paleo-Mesoproterozoic strata in the Priest River region, northwestern USA: A record of Laurentia assembly and Nuna tenure. Precambrian Research 367, 106445.

Brown, D., Pawley, M., Williams, M., Reid, A., Jagodzinski, E., 2022. Zircon LA–ICP–MS geochronology and geochemistry of intrusive rocks from the central-western Gawler Craton, in: Department for Energy and Mining, S.A. (Ed.), Report Book 2022/00008, Adelaide.

Brown, D.A., Morrissey, L.J., Goodge, J.W., Hand, M., 2021. Absence of evidence for Palaeoproterozoic eclogite-facies metamorphism in East Antarctica: no record of subduction orogenesis during Nuna development. Scientific Reports 11, 6717.

Cawood, P.A., Korsch, R.J., 2008. Assembling Australia: Proterozoic building of a continent. Precambrian Research 166, 1–35.

Chalmers, N., 2007. The Mount Woods Domain: a geological review and discussion on mineralisation potential, Report Book 2007/7. Department of Primary Industries and Resources., South Australia.

Cherry, A.R., McPhie, J., Kamenetsky, V.S., Ehrig, K., Keeling, J.L., Kamenetsky, M.B., Meffre, S., Apukhtina, O.B., 2017. Linking Olympic Dam and the Cariewerloo Basin: Was a sedimentary basin involved in formation of the world's largest uranium deposit? Precambrian Research 300, 168–180.

Claoué-Long, J., Edgoose, C., Worden, K., 2008. A correlation of Aileron Province stratigraphy in central Australia. Precambrian Research 166, 230–245.

Collins, W.J., 2002a. Hot orogens, tectonic switching, and creation of continental crust. Geology 30, 535–538.

Collins, W.J., 2002b. Nature of extensional accretionary orogens. Tectonics 21, 6-1-6-12.

Cutts, K., Hand, M., Kelsey, D.E., 2011. Evidence for early Mesoproterozoic (ca. 1590Ma) ultrahigh-temperature metamorphism in southern Australia. Lithos 124, 1–16.

Daly, S.J., Fanning, C.M., Fairclough, M.C., 1998. Tectonic evolution and exploration potential of the Gawler Craton, South Australia. AGSO Journal of Australia Geology and Geophysics 17, 145–168.

Daniel, C.G., Pfeifer, L.S., Jones, J.V., McFarlane, C.M., 2013. Detrital zircon evidence for non-Laurentian provenance, Mesoproterozoic (ca. 1490–1450 Ma) deposition and orogenesis in a reconstructed orogenic belt, northern New Mexico, USA: Defining the Picuris orogeny. Geological Society of America Bulletin 125, 1423–1441.

Del Moro, A., Puxeddu, M., di Brozolo, F.R., Villa, I.M., 1982. Rb-Sr and K-Ar ages on minerals at temperatures of 300°–400° C from deep wells in the Larderello geothermal field (Italy). Contributions to Mineralogy and Petrology 81, 340–349.

Dutch, R., Hand, M., Kinny, P.D., 2008. High-grade Paleoproterozoic reworking in the southeastern Gawler Craton, South Australia. Australian Journal of Earth Sciences 55, 1063–1081.

Dutch, R.A., Hand, M., Kelsey, D.E., 2010. Unravelling the tectonothermal evolution of reworked Archean granulite facies metapelites using in situ geochronology: an example from the Gawler Craton, Australia. Journal of Metamorphic Geology 28, 293–316.

Fanning, C.M., Reid, A.J., Teale, G.S., 2007. A geochronological framework for the Gawler Craton, South Australia, South Australia. Geological Survey. Bulletin 55.

Forbes, C.J., Giles, D., Hand, M., Betts, P.G., Suzuki, K., Chalmers, N., Dutch, R., 2011. Using P-T paths to interpret the tectonothermal setting of prograde metamorphism: An example from the northeastern Gawler Craton, South Australia. Precambrian Research 185, 65–85.

Forbes, C.J., Giles, D., Jourdan, F., Sato, K., Omori, S., Bunch, M., 2012. Cooling and exhumation history of the northeastern Gawler Craton, South Australia. Precambrian Research 200–203, 209–238.

Fraser, G.L., Lyons, P., 2006. Timing of Mesoproterozoic tectonic activity in the northwestern Gawler Craton constrained by 40Ar/39Ar geochronology. Precambrian Research 151, 160–184.

Fraser, G., McAvaney, S., Neumann, N., Szpunar, M., Reid, A., 2010. Discovery of early Mesoarchean crust in the eastern Gawler Craton, South Australia. Precambrian Research 179, 1–21.

Fraser, G., Reid, A., Stern, R., 2012. Timing of deformation and exhumation across the Karari Shear Zone, north-western Gawler Craton, South Australia. Australian Journal of Earth Sciences 59, 547–570.

Fraser, G.L., Skirrow, R.G., Schmidt-Mumm, A., Holm, O., 2007. Mesoproterozoic Gold in the Central Gawler Craton, South Australia: Geology, Alteration, Fluids, and Timing. Economic Geology 102, 1511–1539.

Freeman, H., Tomkinson, M., 2010. Geological setting of iron oxide related mineralisation in the southern Mount Woods Domain, South Australia, in: Porter, T. M. (Ed.), Hydrothermal iron oxide copper-gold & related deposits: A global perspective, pp. 171-190.

Gibson, G.M., Champion, D.C., 2019. Antipodean fugitive terranes in southern Laurentia: How Proterozoic Australia built the American West. Lithosphere 11, 551–559.

Giles, D., Betts, P., Lister, G., 2002. Far-field continental backarc setting for the 1.80–1.67 Ga basins of northeastern Australia. Geology 30, 823–826.

Goodge, J.W., Fanning, C.M., 2016. Mesoarchean and Paleoproterozoic history of the Nimrod Complex, central Transantarctic Mountains, Antarctica: Stratigraphic revisions and relation to the Mawson Continent in East Gondwana. Precambrian Research 285, 242–271.

Hall, J.W., Glorie, S., Reid, A.J., Boone, S.C., Collins, A.S., Gleadow, A., 2018. An apatite U-Pb thermal history map for the northern Gawler Craton, South Australia. Geoscience Frontiers 9, 1293–1308.

Halpin, J.A., Reid, A.J., 2016. Earliest Paleoproterozoic high-grade metamorphism and orogenesis in the Gawler Craton, South Australia: The southern cousin in the Rae family? Precambrian Research 276, 123–144.

Hand, M., Reid, A.J., Jagodzinski, E., 2007. Tectonic Framework and Evolution of the Gawler Craton, Southern Australia. Economic Geology 102, 1377–1395.

Herriott, T.M., Crowley, J.L., Schmitz, M.D., Wartes, M.A., Gillis, R.J., 2019. Exploring the law of detrital zircon: LA-ICP-MS and CA-TIMS geochronology of Jurassic forearc strata, Cook Inlet, Alaska, USA. Geology 47, 1044–1048.

Hogmalm, K.J., Zack, T., Karlsson, A.K.O., Sjöqvist, A.S.L., Garbe-Schönberg, D., 2017. In situ Rb–Sr and K-Ca dating by LA-ICP-MS/MS: an evaluation of N2O and SF6 as reaction gases. Journal of Analytical Atomic Spectrometry 32, 305–313.

Holland, M.E., Karlstrom, K.E., Gehrels, G., Shufeldt, O.P., Begg, G., Griffin, W., Belousova, E., 2018. The Paleoproterozoic Vishnu basin in southwestern Laurentia: Implications for supercontinent reconstructions, crustal growth, and the origin of the Mojave crustal province. Precambrian Research 308, 1–17.

Holland, T.J.B., Powell, R., 2011. An improved and extended internally consistent thermodynamic dataset for phases of petrological interest, involving a new equation of state for solids. Journal of Metamorphic Geology 29, 333–383.

Holm, O., 2004. New geochronology of the Mount Woods Inlier and the central Gawler gold province, Gawler Craton: State of Play 2004. Department of Primary Industries and Resources, South Australia, Report Book.

Howard, K.E., Hand, M., Barovich, K.M., Payne, J.L., Belousova, E.A., 2011a. U-Pb, Lu–Hf and Sm–Nd isotopic constraints on provenance and depositional timing of metasedimentary rocks in the western Gawler Craton: Implications for Proterozoic reconstruction models. Precambrian Research 184, 43–62.

Howard, K.E., Hand, M., Barovich, K.M., Payne, J.L., Cutts, K.A., Belousova, E.A., 2011b. U-Pb zircon, zircon Hf and whole-rock Sm–Nd isotopic constraints on the evolution of Paleoproterozoic rocks in the northern Gawler Craton. Australian Journal of Earth Sciences 58, 615–638.

Jackson, S.E., Pearson, N.J., Griffin, W.L., Belousova, E.A., 2004. The application of laser ablation-inductively coupled plasma-mass spectrometry to in situ U-Pb zircon geochronology. Chemical Geology 211, 47–69.

Jagodzinski, E., 2005. Compilation of SHRIMP U-Pb geochronological data: Olympic Domain, Gawler Craton, South Australia 2001–2003. Geoscience Australia 197.

Jagodzinski, E.A., Reid, A., 2017. PACE Geochronology: Results of Collaborative Geochronology Projects 2013-2015. Department of the Premier and Cabinet.

Jagodzinski, E., Black, L., Frew, R., Foudoulis, C., Reid, A., Payne, J., Zang, W., Schwarz, M., 2006. Compilation of SHRIMP U-Pb geochronological data for the Gawler

Craton, South Australia 2005-2006. Primary Industries and Resources South Australia Report Book 20.
Jagodzinski, E.A., Reid, A.J., Chalmers, N., Swain, G., Frew, R.A., Foudoulis, C., 2007. Compilation of SHRIMP U-Pb geochronological data for the Gawler Craton, South Australia, 2007, South Australian Department of Primary Industries and Resources, Report Book 2007/21.
Jagodzinski, E.A., Reid, A.J., Crowley, J.L., Wade, C.E., Curtis, S., 2023. Precise zircon U-Pb dating of the Mesoproterozoic Gawler large igneous province. South Australia. Results in Geochemistry 10, 100020.
Jenkin, G.R.T., Ellam, R.M., Rogers, G., Stuart, F.M., 2001. An investigation of closure temperature of the biotite Rb-Sr system: The importance of cation exchange. Geochimica et Cosmochimica Acta 65, 1141–1160.
Kelly, N.M., Clarke, G.L., Harley, S.L., 2006. Monazite behaviour and age significance in poly-metamorphic high-grade terrains: A case study from the western Musgrave Block, central Australia11Abbreviations: After Kretz, 1983. Lithos 88, 100–134.
Kirscher, U., Mitchell, R.N., Liu, Y., Nordsvan, A.R., Cox, G.M., Pisarevsky, S.A., Wang, C., Wu, L., Murphy, J.B., Li, Z.-X., 2020. Paleomagnetic constraints on the duration of the Australia-Laurentia connection in the core of the Nuna supercontinent. Geology 49, 174–179.
Kohn, M.J., Malloy, M.A., 2004. Formation of monazite via prograde metamorphic reactions among common silicates: implications for age determinations. Geochimica et Cosmochimica Acta 68, 101–113.
Kröner, A., Braun, I., Jaeckel, P., 1996. Zircon geochronology of anatectic melts and residues from a highgrade pelitic assemblage at Ihosy, southern Madagascar: evidence for Pan-African granulite metamorphism. Geological Magazine 133, 311–323.
Lane, K., Jagodzinski, E.A., Dutch, R., Reid, A.J., Hand, M., 2015. Age constraints on the timing of iron ore mineralisation in the southeastern Gawler Craton. Australian Journal of Earth Sciences 62, 55–75.
De Vries Van Leeuwen, A.T., Morrissey, L.J., Raimondo, T., Hand, M., 2022. Prolonged high thermal gradient metamorphism in the Curnamona Province, south-central Australia, during the latter stages of Nuna assembly. Precambrian Research 378, 106775.
Ludwig, K., 2012. Isoplot 4.15: a geochronological toolkit for Microsoft Excel. Berkeley Geochronology Center Special. Publication 5.
Maidment, D.W., 2005. Palaeozoic high-grade metamorphism within the Centralian Superbasin, Harts Range region, central Australia. Australian National University, Canberra, p. 422.
McFarlane, C.R.M., 2006. Palaeoproterozoic evolution of the Challenger Au deposit, South Australia, from monazite geochronology. Journal of Metamorphic Geology 24, 75–87.
McLaren, S., Sandiford, M., Hand, M., Neumann, N., Wyborn, L., Bastrakova, I., 2003. The hot southern continent: heat flow and heat production in Australian Proterozoic terranes. Geological Society of America Special Papers 372, 157–167.
Medig, K.P.R., Thorkelson, D.J., Davis, W.J., Rainbird, R.H., Gibson, H.D., Turner, E.C., Marshall, D.D., 2014. Pinning northeastern Australia to northwestern Laurentia in the Mesoproterozoic. Precambrian Research 249, 88–99.
Morrissey, L.J., Hand, M., Wade, B.P., Szpunar, M., 2013. Early Mesoproterozoic metamorphism in the Barossa Complex, South Australia: links with the eastern margin of Proterozoic Australia. Australian Journal of Earth Sciences 60, 769–795.
Morrissey, L.J., Hand, M., Kelsey, D.E., Wade, B.P., 2016a. Cambrian high-temperature reworking of the Rayner-Eastern Ghats terrane, constraints from the northern Prince Charles Mountains region, east Antarctica. Journal of Petrology 57, 53–92.
Morrissey, L.J., Hand, M., Lane, K., Kelsey, D.E., Dutch, R.A., 2016b. Upgrading iron-ore deposits by melt loss during granulite facies metamorphism. Ore Geology Reviews 74, 101–121.
Morrissey, L.J., Barovich, K.M., Hand, M., Howard, K.E., Payne, J.L., 2019. Magmatism and metamorphism at ca. 1.45 Ga in the northern Gawler Craton: the Australian record of rifting within Nuna (Columbia). Geoscience Frontiers 10, 175–194.
Olierook, H.K.H., Rankenburg, K., Ulrich, S., Kirkland, C.L., Evans, N.J., Brown, S., McInnes, B.I.A., Prent, A., Gillespie, J., McDonald, B., Darragh, M., 2020. Resolving multiple geological events using in situ Rb–Sr geochronology: implications for metallogenesis at Tropicana, Western Australia. Geochronology 2, 283–303.
Olierook, H.K.H., Mervine, E.M., Armstrong, R., Duckworth, R., Evans, N.J., McDonald, B., Kirkland, C.L., Shantha Kumara, A., Wood, D.G., Cristall, J., Jhala, K., Stirling, D.A., Friedman, I., McInnes, B.I.A., 2022. Uncovering the Leichhardt Superbasin and Kalkadoon-Leichhardt Complex in the southern Mount Isa Terrane. Australia. Precambrian Research 375, 106680.
Paton, C., Woodhead, J.D., Hellstrom, J.C., Hergt, J.M., Greig, A., Maas, R., 2010. Improved laser ablation U-Pb zircon geochronology through robust downhole fractionation correction. Geochemistry, Geophysics, Geosystems 11, 1–36.
Paton, C., Hellstrom, J., Paul, B., Woodhead, J., Hergt, J., 2011. Iolite: Freeware for the visualisation and processing of mass spectrometric data. Journal of Analytical Atomic Spectrometry 26, 2508–2518.
Payne, J.L., Barovich, K., Hand, M., 2006. Provenance of metasedimentary rocks in the northern Gawler Craton, Australia: Implications for Palaeoproterozoic reconstructions. Precambrian Research 148, 275–291.
Payne, J.L., Hand, M., Barovich, K.M., Wade, B.P., 2008. Temporal constraints on the timing of high-grade metamorphism in the northern Gawler Craton: implications for assembly of the Australian Proterozoic. Australian Journal of Earth Sciences 55, 623–640.
Payne, J.L., Hand, M., Barovich, K.M., Reid, A., Evans, D.A.D., 2009. Correlations and reconstruction models for the 2500–1500 Ma evolution of the Mawson Continent. Geological Society, London, Special Publications 323, 319–355.
Payne, J.L., Ferris, G., Barovich, K.M., Hand, M., 2010. Pitfalls of classifying ancient magmatic suites with tectonic discrimination diagrams: An example from the Paleoproterozoic Tunkillia Suite, southern Australia. Precambrian Research 177, 227–240.
Payne, J.L., Morrissey, L.J., Tucker, N.M., Roche, L.K., Szpunar, M.A., Neroni, R., 2021. Granites and gabbros at the dawn of a coherent Australian continent. Precambrian Research 359, 106189.
Pehrsson, S.J., Eglington, B.M., Evans, D.A.D., Huston, D., Reddy, S.M., 2015. Metallogeny and its link to orogenic style during the Nuna supercontinent cycle, in: Li, Z.X., Evans, D.A.D., Murphy, J.B. (Eds.), Supercontinent Cycles Through Earth History. Geological Society, London, Special Publications, pp. 83-94.
Peucat, J.J., Capdevila, R., Fanning, C.M., Ménot, R.P., Pécora, L., Testut, L., 2002. 1.60 Ga felsic volcanic blocks in the moraines of the Terre Adélie Craton, Antarctica: Comparisons with the Gawler Range Volcanics, South Australia. Australian Journal of Earth Sciences 49, 831–845.
Pisarevsky, S.A., Elming, S.-Å., Pesonen, L.J., Li, Z.-X., 2014. Mesoproterozoic paleogeography: Supercontinent and beyond. Precambrian Research 244, 207–225.
Pourteau, A., Smit, M.A., Li, Z.-X., Collins, W.J., Nordsvan, A.R., Volante, S., Li, J., 2018. 1.6 Ga crustal thickening along the final Nuna suture. Geology 46, 959–962.
Powell, R., White, R.W., Green, E.C.R., Holland, T.J.B., Diener, J.F.A., 2014. On parameterizing thermodynamic descriptions of minerals for petrological calculations. Journal of Metamorphic Geology 32, 245–260.
Rankenburg, K., Lassiter, J.C., Brey, G., 2004. Origin of megacrysts in volcanic rocks of the Cameroon volcanic chain – constraints on magma genesis and crustal contamination. Contributions to Mineralogy and Petrology 147, 129–144.
Redaa, A., Farkaš, J., Gilbert, S., Collins, A.S., Wade, B., Löhr, S., Zack, T., Garbe-Schönberg, D., 2021. Assessment of elemental fractionation and matrix effects during in situ Rb–Sr dating of phlogopite by LA-ICP-MS/MS: implications for the accuracy and precision of mineral ages. Journal of Analytical Atomic Spectrometry 36, 322–344.
Reid, A., Forster, M., 2021. Mesoproterozoic thermal evolution of the northern Gawler Craton from 40Ar/39Ar geochronology. Precambrian Research 358, 106180.
Reid, A.J., Halpin, J.A., Dutch, R.A., 2019. Timing and style of high-temperature metamorphism across the Western Gawler Craton during the Paleo- to Mesoproterozoic. Australian Journal of Earth Sciences 66, 1085–1111.
Reid, A., Hand, M., Jagodzinski, E., Kelsey, D., Pearson, N., 2008. Paleoproterozoic orogenesis in the southeastern Gawler Craton, South Australia. Australian Journal of Earth Sciences 55, 449–471.
Reid, A.J., Hand, M., 2012. Mesoarchean to Mesoproterozoic evolution of the southern Gawler Craton, South Australia. Episodes 35, 216–225.
Reid, A.J., Jagodzinski, E.A., Armit, R.J., Dutch, R.A., Kirkland, C.L., Betts, P.G., Schaefer, B.F., 2014a. U-Pb and Hf isotopic evidence for Neoarchean and Paleoproterozoic basement in the buried northern Gawler Craton, South Australia. Precambrian Research 250, 127–142.
Reid, A.J., Jagodzinski, E.A., Fraser, G.L., Pawley, M.J., 2014b. SHRIMP U-Pb zircon age constraints on the tectonics of the Neoarchean to early Paleoproterozoic transition within the Mulgathing Complex, Gawler Craton, South Australia. Precambrian Research 250, 27–49.
Reid, A.J., Jagodzinski, E.A., Wade, C.E., Payne, J.L., Jourdan, F., 2017. Recognition of c. 1780Ma magmatism and metamorphism in the buried northeastern Gawler Craton: Correlations with events of the Aileron Province. Precambrian Research 302, 198–220.
Reid, A.J., Pawley, M.J., Wade, C., Jagodzinski, E.A., Dutch, R.A., Armstrong, R., 2020. Resolving tectonic settings of ancient magmatic suites using structural, geochemical and isotopic constraints: the example of the St Peter Suite, southern Australia. Australian Journal of Earth Sciences 67, 31–58.
Reid, A., 2013. Reconnaissance LA-ICPMS zircon U-Pb geochronology from samples from the centralnorthern Gawler Craton, Report Book 2013/00021. Department for Manufacturing, Innovation, Trade, Resources and Energy, South Australia, Adelaide.
Ross, G.M., Villeneuve, M., 2003. Provenance of the Mesoproterozoic (1.45 Ga) Belt basin (western North America): Another piece in the pre-Rodinia paleogeographic puzzle. Geological Society of America Bulletin 115, 1191–1217.
Scibiorski, E., Jourdan, F., Mezger, K., Tohver, E., Vollstaedt, H., 2021. Cryptic excess argon in metamorphic biotite: Anomalously old 40Ar/39Ar plateau dates tested with Rb/Sr thermochronology and Ar diffusion modelling. Geochimica et Cosmochimica Acta 315, 1–23.
Scrimgeour, I.R., 2013. Chapter 12: Aileron Province, in: Ahmad, M., Munson, T.J. (Eds.), Geology and mineral resources of the Northern Territory. Northern Territory Geological Survey.
Skirrow, R., Bastrakov, E., Barovich, K., Fraser, G., Creaser, R.A., Fanning, C.M., Raymond, O., Davidson, G.J., 2007. Timing of Iron Oxide Cu-Au-(U) Hydrothermal Activity and Nd Isotope Constraints on Metal Sources in the Gawler Craton, South Australia. Economic Geology 102, 1441–1470.
Sláma, J., Košler, J., Condon, D.J., Crowley, J.L., Gerdes, A., Hanchar, J.M., Horstwood, M.S., Morris, G.A., Nasdala, L., Norberg, N., 2008. Plešovice zircon—a new natural reference material for U-Pb and Hf isotopic microanalysis. Chemical Geology 249, 1–35.
Swain, G., Woodhouse, A., Hand, M., Barovich, K., Schwarz, M., Fanning, C.M., 2005. Provenance and tectonic development of the late Archaean Gawler Craton, Australia; U-Pb zircon, geochemical and Sm–Nd isotopic implications. Precambrian Research 141, 106–136.
Swain, G., Barovich, K., Hand, M., Ferris, G., Schwarz, M., 2008. Petrogenesis of the St Peter Suite, southern Australia: Arc magmatism and Proterozoic crustal growth of the South Australian Craton. Precambrian Research 166, 283–296.
Szpunar, M., Hand, M., Barovich, K., Jagodzinski, E., Belousova, E., 2011. Isotopic and geochemical constraints on the Paleoproterozoic Hutchison Group, southern Australia: Implications for Paleoproterozoic continental reconstructions. Precambrian Research 187, 99–126.

Tiddy, C.J., Betts, P.G., Neumann, M.R., Murphy, F.C., Stewart, J., Giles, D., Sawyer, M., Freeman, H., Jourdan, F., 2020. Interpretation of a ca. 1600–1580 Ma metamorphic core complex in the northern Gawler Craton. Australia. Gondwana Research 85, 263–290.

Vassallo, J.J., Wilson, C.J.L., 2002. Palaeoproterozoic regional-scale non-coaxial deformation: an example from eastern Eyre Peninsula, South Australia. Journal of Structural Geology 24, 1–24.

Vermeesch, P., 2018. IsoplotR: A free and open toolbox for geochronology. Geoscience Frontiers 9, 1479–1493.

Volante, S., Pourteau, A., Collins, W.J., Blereau, E., Li, Z.-X., Smit, M., Evans, N.J., Nordsvan, A.R., Spencer, C.J., McDonald, B.J., Li, J., Günter, C., 2020. Multiple P-T–d–t paths reveal the evolution of the final Nuna assembly in northeast Australia. Journal of Metamorphic Geology 38, 593–627.

Volante, S., Collins, W.J., Barrote, V., Nordsvan, A.R., Pourteau, A., Li, Z.X., Li, J., Beams, S., 2022. Spatio–temporal evolution of Mesoproterozoic magmatism in NE Australia: A hybrid tectonic model for final Nuna assembly. Precambrian Research 372, 106602.

Wade, C.E., McAvaney, S., 2017. Stratigraphy and geochemistry of the 1745-1700 Ma Peter Pan Supersuite. Department of State Development.

Wade, C.E., Reid, A.J., Wingate, M.T.D., Jagodzinski, E.A., Barovich, K., 2012. Geochemistry and geochronology of the c. 1585Ma Benagerie Volcanic Suite, southern Australia: Relationship to the Gawler Range Volcanics and implications for the petrogenesis of a Mesoproterozoic silicic large igneous province. Precambrian Research 206–207, 17–35.

Webb, A.W., Thomson, B.P., Blissett, A.H., Daly, S.J., Flint, R.B., Parker, A.J., 1986. Geochronology of the Gawler Craton, South Australia. Australian Journal of Earth Sciences 33, 119–143.

White, R.W., Powell, R., Holland, T.J.B., Johnson, T.E., Green, E.C.R., 2014a. New mineral activity–composition relations for thermodynamic calculations in metapelitic systems. Journal of Metamorphic Geology 32, 261–286.

White, R.W., Powell, R., Johnson, T.E., 2014b. The effect of Mn on mineral stability in metapelites revisited: new a–x relations for manganese-bearing minerals. Journal of Metamorphic Geology 32, 809–828.

Wiedenbeck, M., Alle, P., Corfu, F., Griffin, W., Meier, M., Oberli, F.v., Quadt, A.v., Roddick, J., Spiegel, W., 1995. Three natural zircon standards for U-Th-Pb, Lu-Hf, trace element and REE analyses. Geostandards and Geoanalytical Research 19, 1-23.

Williams, M.L., Jercinovic, M.J., Harlov, D.E., Budzyn, B., Hetherington, C.J., 2011. Resetting monazite ages during fluid-related alteration. Chemical Geology 283, 218–225.

Williams, M.A., Kelsey, D.E., Hand, M., Raimondo, T., Morrissey, L.J., Tucker, N.M., Dutch, R.A., 2018. Further evidence for two metamorphic events in the Mawson Continent. Antarctic Science 30, 44–65.

Woodhead, J.D., Hergt, J.M., 2001. Strontium, neodymium and lead isotope analyses of NIST glass certified reference materials: SRM 610, 612, 614. Geostandards Newsletter 25 (2–3), 261–266.

Yakymchuk, C., 2017. Behaviour of apatite during partial melting of metapelites and consequences for prograde suprasolidus monazite growth. Lithos 274–275, 412–426.

Yakymchuk, C., Brown, M., Clark, C., Korhonen, F.J., Piccoli, P.M., Siddoway, C.S., Taylor, R.J.M., Vervoort, J.D., 2015. Decoding polyphase migmatites using geochronology and phase equilibria modelling. Journal of Metamorphic Geology 33, 203–230.

Zack, T., Hogmalm, K.J., 2016. Laser ablation Rb/Sr dating by online chemical separation of Rb and Sr in an oxygen-filled reaction cell. Chemical Geology 437, 120–133.